Title

Hybridizing clinical translatability with enzyme-free DNA signal amplifiers: recent advances in nucleic acid detection and imaging

Journal

Biomaterials Science, 9(2)

ISSN

2047-4830

Authors

Borum, Raina M
Jokerst, Jesse V

Publication Date

2021-01-21

DOI

10.1039/d0bm00931h

Peer reviewed

Published in final edited form as:

Biomater Sci. 2021 January 21; 9(2): 347–366. doi:10.1039/d0bm00931h.

Hybridizing clinical translatability with enzyme-free DNA signal amplifiers: recent advances in nucleic acid detection and imaging

Raina M. Borum[a], **Jesse V. Jokerst**[a,b,c]

[a]Department of NanoEngineering, University of California, San Diego, 9500 Gilman Drive, La Jolla, California, 92093 USA

[b]Materials Science and Engineering Program, University of California, San Diego, 9500 Gilman Drive, La Jolla, CA, 92093, USA

[c]Department of Radiology, University of California, San Diego, 9500 Gilman Drive, La Jolla, CA 92093, USA

Abstract

Nucleic acid species have become a viable prognostic and diagnostic biomarker for a diverse class of diseases, particularly cancer. However, the low femtomolar to attomolar concentration of nucleic acids in human samples require sensors with excellent detection capabilities; many past and current platforms fall short or are economically difficult. Strand-mediated signal amplifiers such as hybridization chain reaction (HCR) and catalytic hairpin assembly (CHA) are superior methods for detecting trace amounts of biomolecules because one target molecule triggers the continuous production of synthetic double-helical DNA. This cascade event is highly discriminatory to the target via sequence specificity, and it can be coupled with fluorescence, electrochemistry, magnetic moment, and electrochemiluminescence for signal reporting. Here, we review recent advances in enhancing the sensing abilities in HCR and CHA including improved live-cell imaging efficiency, lowered limit of detection, and optimized multiplexity. We further outline the potential for clinical translatability of HCR and CHA by summarizing progress in employing these two tools for *in vivo* imaging, human sample testing, and sensing-treating dualities. We finally discuss their future prospects and suggest clinically-relevant experiments to supplement further related research.

Graphical Abstract

Conflicts of interest

There are no conflicts to declare.

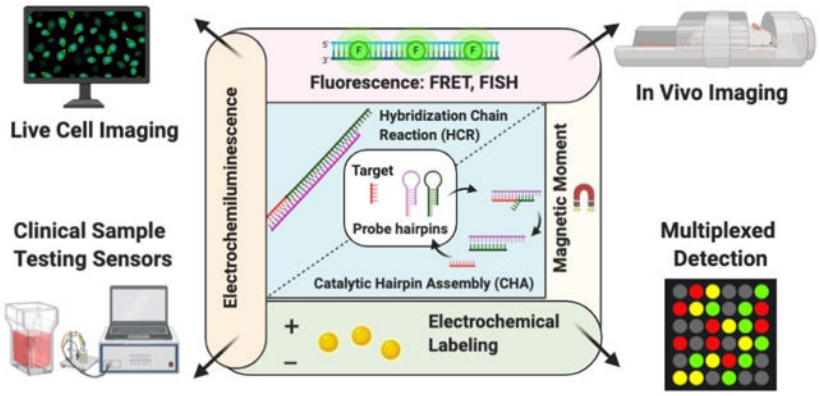

Strand amplifying HCR and CHA are adaptable with signalers for novel and clinically translatable nucleic acid sensors and imaging agents.

Introduction

An extensive variety of RNA and DNA molecules are characteristically under or over-expressed in many diseases[1]. Although discovered in 1948[2], extracellular nucleic acids were first correlated to disease nearly 40 years later[3,69] when their overexpression was seen in the serum of cancer patients. Similarly, heightened intracellular abundance of signature nucleic acids in vesicles and exosomes has been observed in metastatic cell lines[115]. Now, the abnormal regulation of diversified functional nucleic acids— such as intracellular, noncoding, circulating, and even genomic species—is a hallmark for the presence and progression of cancers, diabetes, stroke, and cardiovascular diseases[99]. Nucleic acid biomarkers' particular relation to cancer involves their release from lysed tumor cells into plasma[1] as well as their exosomal transfer between cells[116]. Species such as messenger RNA (mRNA), cell-free DNA (cfDNA), and microRNA (miRNA) are some the most notable disease footprints[73]. miRNA is a particularly popular marker because it is short (~22nt) to sequence and is stable in serum[4,74]. miRNA concentrations can also predict survival time in cancer[75].

Opportunities from standardized nucleic acid profiling are as versatile as they are novel: examples include early stage diagnosis, accurate surveillance after cancer remission or ongoing therapy, nucleic acid species-specific mapping between disease variants, or refined prognosis and estimated survival. Furthermore, circulating nucleic acids are characteristically present in plasma[5,67], serum[3,5,75], saliva[68,70], urine,[67,71] sputum/pleural effusions[52,72], and tissue based on the location and nature of the disease. Nucleic acid species are therefore attractive targets for sensitive, economic, and time-efficient liquid biopsies.

Current gold standards for nucleic acid detection include northern blotting, microarrays, and quantitative reverse transcription PCR[1,66], but these tools are expensive and time-consuming. qRT-PCR particularly suffers from dubious RNA sequencing accuracy because the required primers generate multiple complimentary DNA strands from the original sequence either (1) in a nonspecific manner thus reducing quantification accuracy or (2) in a

wasteful way such that separate reactions are required for each primer. This makes it unsuitable for samples with low abundant targets[86]. Nanotechnology strategies include DNA-grafted gold nanoparticles for fluorescent imaging of live cells[114] based on miRNA and mRNA recognition, but this falls short to a required dense input probe concentration and is therefore not as practical for clinical diagnosis applications. These related platforms also lack signal amplification, so their sensitivity remains inferior to other methods such as qtPCR.

Strand amplification—the continuous generation of nucleic acid strands upon an event such as hybridization with a target nucleic acid—is a provocative idea to detect trace amounts of nucleic acid. The ability to sense native nucleic acid with synthetic nucleic acid is biocompatible, safe, nanoscale, and noninvasive. The ability to functionalize synthetic nucleic acids with dyes, proteins, nanoparticles, and chemical reporters is standardized and well-defined[89,90] thus offering pragmatic translatability for clinical imaging and liquid biopsies. For example, rolling circle amplification (RCA) is a robust method to indefinitely produce single-stranded (ss)DNA by enzymatic cycling through a circular template ssDNA. RCA can therefore mass produce DNA upon endogenous nucleic acid detection[61], but the required DNA polymerase and ligase limit the platform for *in vivo* applications. RCA also requires thermocycling to enable hybridization and amplification deactivation, further limiting its use beyond the benchtop. Though thoroughly practiced, this high-maintenance platform has limited candidacy in realistic diagnostic applications—particularly *in vivo* applications.

The advent of enzyme-free and isothermal strand amplification, as pioneered by Pierce in the early 2000s[6,7], completely reshaped the landscape of DNA amplification. Here, hybridization between nucleic acid strands could trigger continuous DNA production without external events or entities. These engineered amplification methods typically use hybridization chain reaction (HCR) and catalytic hairpin assembly (CHA); both have exceptionally detection limits while yielding synthetic DNA for a characteristic readout. HCR and CHA both require a “fuel strand”—the target analyte—to hybridize with synthetic nucleic acid strands that catalyze the indefinite growth of artificial DNA molecules. HCR and CHA fundamentally require only two strand species and one fuel strand to trigger the programmed cascades; therefore, they have inherently low limits of detection and high specificity. This makes them ideal candidates for nucleic acid detection and disease profiling.

In this review, we examine recent milestones achieved by HCR and CHA that bring them closer to clinical applications, with an emphasis on diagnostic and prognostic devices as well as nucleic acid mapping via *in vivo* imaging. We outline advances in three key areas: (1) enhancements in live cell imaging, (2) designs with very low detection limits (attomolar range), and (3) multiplexed sensing abilities. We further report recent progress in utilizing these methods in pragmatic clinical use including demonstrations of *in vivo* imaging, nucleic acid sensing in human samples, and theranostics.

Principles of Strand Amplification

Strand amplification is an inviting approach to amplify signals for nucleic acid sensors that require low detection limits. In general, they yield either (1) a large output of synthetically duplexed DNA or (2) constant cycling of duplex formation or strand exchange upon recognition of one target strand. Toehold-mediated strand displacement (TMSD) is a DNA programming tool that has ultimately enabled enzyme-free signal amplification; in this approach, recognition of one target strand results in a product strand or duplex[97]. In TMSD, the toehold—or exposed target recognition region for hybridization—is concealed until the target is present. One way to execute this is by kinetically trapping the target recognition sequence in DNA hairpins[98]. TMSD has resulted in powerful logic gates, machines, motors, and programmed events on the molecular scale. Two such DNA programming tools that have powerfully utilized TMSD for pragmatic nucleic acid sensing include hybridization chain reaction (HCR) and catalytic hairpin assembly (CHA)[103,104].

Hybridization Chain Reaction (HCR)

In hybridization chain reaction ((Figure 1A), one target strand serves as fuel to activate the continuous growth of nicked concatemers[6]. Two uniquely-sequenced HCR strands initially store potential energy as metastable hairpin loops in the “OFF state.” Upon contact with the fuel strand, strand type 1 will open from its hairpin state into a single stranded “ON state”, partially hybridizing with the fuel strand while simultaneously hybridizing with strand type 2. The remaining region in strand type 2—which is identical to the fuel strand sequence—enforces the cascade by retriggering hybridization with the beginning of a new strand type **1** (Figure 1A). This results in indefinite growth of a double helical superstructure until hairpin supply is depleted. The total molecular weight of the HCR product has an inverse relationship with the starter fuel strand concentration[6]. Since its first demonstration in 2004 by Dirks and Pierce[6], HCR has become the foundation of strand amplification engineering. The earliest studies on HCR demonstrate impressive *in situ* RNA mapping in zebrafish embryo samples[9], but serious drawbacks from required sample preparation and strand washing have restrained the platform from immediate clinical utility. Live cell imaging was at first impossible because the cells required further pre-treatment such as fixation and cycled washing of unhybridized probes. Still, their mapping demonstrations proved 200-fold sensitivity from HCR above unamplified hybridization fluorescence.

Catalytic Hairpin Assembly (CHA)

A close relative to HCR is catalytic hairpin assembly (CHA), an entropy-driven[112] catalysis reaction which was also invented by Pierce’s group in 2008[7]. The mechanism is comparable to HCR in the sense that two metastable hairpin loops are stimulated for duplex formation upon fuel strand recognition. However, as the fuel strand hybridizes with the first probe, it is released to allow further assembly between the first and second probes for accumulated production of discretized, short duplexes (Figure 1B). This provides an advantage over HCR because the target strand can be continuously recycled, decreasing the cascade reaction time and generating “100-fold signal amplification in a few hours.” [8]

Improvements in Live Cell Imaging

Signal amplification from HCR and CHA often use fluorescent dyes tethered to the strands. These fluorescent methods typically utilize (1) fluorescent *in situ* hybridization (FISH) where the hybridization between two strands leads to the excitation of a dye molecule upon incident light; or (2) Förster Resonance Energy Transfer (FRET) where distance-dependent dye-quencher or dye-dye pairs are within sufficient proximity to transfer excitation energy between each other. With these techniques, HCR and CHA have consistently demonstrated unprecedented nucleic acid imaging in cells while precisely preserving spatial expression; this has exhibited striking patterns of different RNA species across the same tissue sample[9-10,12]. HCR first mapped mRNA patterns in zebrafish embryos in 2010[9], but only imaged live cells in 2015 after grafting fluorescent HCR probes onto gold nanoparticle carriers[11]. Since then, major developments have strengthened imaging quality and efficiency in live cells.

One ultimate goal with live cell imaging is graduation to robust *in vivo* imaging. While *in vivo* visualization of nucleic acid has never been seriously explored, HCR and CHA can give clinicians the power to observe nucleic acid patterns within live tissue for a more localized understanding of disease markers. Spatial monitoring of tell-tale nucleic acids is also an appealing method to gather clues on a developing disease while elucidating survival. To advance HCR and CHA from *in vitro* to *in vivo* imaging, (1) visualization, (2) biostability and biocompatibility, as well as (3) target diversity must be optimized[94].

Visualization Improvements

Outstanding advances in HCR and CHA-mediated imaging include enhancing contrast, reducing background, and expediting required imaging time. A notable contribution to these efforts comes from Pierce's “Third Generation HCR” in 2018.[12] One problem with the original HCR was nonspecific binding between the HCR probes and random nucleic acids, which result in heightened background fluorescence and signal leakage[12-13]. Third Generation HCR overcomes this problem by replacing the first amplification probe with two “split-initiator probes;” these split initiators carry only half of the original amplification strand (Figure 2A). In order to gather the correct signal, the target strand must hybridize with *both* split initiators before cascading. This method therefore coerces more rigorous sequence specificity to suppress nonspecific background. (Figure 2B).

A critical goal in fluorescent-probed strand amplification is coherent and spatial imaging of the targets in live cells. In this regard, creating imaging contrast between areas of different nucleic acid distributions has been a hurdle. CHA mechanisms particularly suffer from reduced contrast because target strand recycling only produces discrete duplexes rather than individual duplex superstructures. Consequently, traditional CHA products have scattered and sparse fluorescence—regardless of how many duplexes are produced—which reduces contrast and CHA’s inherent imaging viability. Huang et al. directly address this limitation by designing CHA probes that form crosslinking tetrads upon mRNA (survivin or TK1) recognition[14]. The produced superstructures generated meshes that consolidate fluorescent signals for significant contrast improvements over traditional CHA. In fact, traditional CHA

resulted in structures on the order of tens of nanometers while the crosslinked CHA meshes were several hundred nanometers at identical starting concentrations.

Another key challenge in strand amplification imaging is the required time to yield distinguishable fluorescence. Most HCR and CHA techniques need several hours for sufficient signal output (Table 1)[9,10]. The first demonstration of *in situ* HCR imaging required about 36 hours to effectively map RNA in embryo samples[9] but progress has reduced the reaction time to one to two hours in live cells (Table 1). While many works demonstrate such reduced times, the various approaches were made to achieve different goals while collaterally addressing this issue; for example, helper-delivery nanoparticles and secondary DNA structures contributed to these 1-2hr reaction times. Reports from the past year, however, show that 3D DNA probes dependably accelerate the reaction time. Wang et al.'s work with HCR demonstrated observable fluorescence in an impressive 20 minutes[15]. The amplification kinetics were hastened by 3D tetrahedral DNA structures. Key advantages to this architecture include (1) enabled quadrivalency in hybridization sites at the tetrahedron vertices and (2) increased local concentration of reaction sites for HCR to occur (Figure 2C). Not only did this improve the reaction time 70-fold versus traditional HCR, but it generated micron-ranged superstructures that provide clearer, brighter, and more coherent fluorescence. (Figure 2D) CHA was similarly re-designed for heightened reaction speed. Qing et al. similarly utilized 3D tetrahedrons to improve CHA reaction kinetics; this same approach reduced the time for a sufficient signal-to-noise ratio from 48 minutes to only 3 minutes[16].

Higher order DNA structures can therefore decrease reaction time and increase contrast, but the works above do not show any demonstrations in a whole animal; future work invites the incorporation of these design strategies in a mouse model. It would be imperative to corroborate the sustainability of heightened reaction time and enhanced contrast in a living system. One can also couple Third Generation HCR with higher order DNA structures to avoid background fluorescence during imaging.

Diversity of molecular target imaging

Besides nucleic acids, DNA and RNA have high affinity to proteins through characteristic binding interactions, and their standardized covalent labeling with reactive organic groups expands their avidity to a wider class of entities[55]; by chemically linking single strands with other molecules such as peptides and click-chemistry actors, nucleic acid possesses the unique potential to image diversified targets on the nanoscale.

Aptamers are structural nucleic acids with high specificity to a wide range of biomolecular species and possess binding strengths that are analogous to the antibody-protein model. These secondary structured nucleic acids install themselves along grooves and reactive sites with K_D values in the nanomolar to as low as picomolar range[17,88]. Aptamers are therefore coupled with strand amplification to minimize the required concentration of target protein analytes. Qin et al. utilized an aptamer-embedded hairpin and two additional hairpin probe species to form HCR-networked superstructures upon cytokine sensing[18]. Their target fuel-protein, IFN-γ, first hybridizes with the aptamer probe, elongating the remainder ofthe strand to hybridize with hairpin 2. Hairpin 2 is allowed to bind with the aptamer probe in

two different orientations, leading to two different aptamer-hairpin 2 products. Similarly, the multiple conformations of hairpin 3 re-exposes binding points for hairpin 2, accommodating two different aptamer-hairpin2-hairpin3 products. When hairpin 2 binds with these diverse products, the hierarchical network continuously grows (Figure 3A). This simple mechanism competes with current standards in IFN-γ sensing—primarily immunological assays—which are costly and laborious. Besides triggered hierarchical assembly, aptamer-HCR has been implemented in other ways such as by Boolean-mediated HCR circuits for the "smart sensing" of two protein species[18].

The good compatibility of nucleic acids with other molecular species has enabled HCR and CHA to effectively detect other endogenous targets (Table 1). Strand-induced signal amplification has monitored cytokines, sialic acid species[85], and specific glycosylation events across cell membranes[55,87]. In fact, the prevalence of cell free proteins and other biomolecules welcome molecular programming tools like strand amplification to enable highly sensitive bioimaging.

Stability to and within live cells

The stability and safety of strand amplification in live cells are equally crucial during experimental design. Synthetic nucleic acids are unstable against the rich abundance of RNAse, DNAse, and other nucleases within cytoplasmic and extracellular space. Consequently, most synthetic nucleic acids are digested within several minutes while higher-order DNA nanostructures inevitably undergo structural denaturation[20]. Furthermore, their negatively-charged phosphate backbone makes it difficult for them to surpass the cell membrane alone. Besides these weaknesses in nucleic acid, live-cell imaging methods require a light source that will not collaterally damage skin, cells, and tissue. Thus, (1) near ultraviolet (UV) sources must be avoided, (2) nucleic acid chemical and structural modifications should be investigated for heightened stability, and (3) inert delivery of the probes to the designated target should be thoroughly explored. Because HCR requires at least one to a few hours for a signal, probes should be designed to withstand at least four to five hours for practical *in vivo* applications.

Chu et al. addressed all of these issues by grafting HCR hairpin probes onto lanthanide ion-doped upconverting nanoparticles (UCNPs) to guide delivery and deliberately activate HCR[21]. Not only do the UCNPs act as a vehicle to ensure hairpin delivery, but they also serve as a safe source to ignite the HCR reaction by presenting the target region of the hairpin only when necessary (Figure 4A). UCNPs are chemically engineered nanoparticles whose crystal asymmetry accelerates a near infrared (NIR) source wavelength to a UV output wavelength. Incident NIR translates into UV light when the HCR hairpins are grafted onto the UCNPs. This breaks a photocleavable crosslinker embedded in the hairpins and exposes them to their target once inside the cell. This controllable activation led to c-MYC mRNA-based HCR with superb spatial and temporal resolution. The system only required a harmless 980 nm light source.

Manganese oxide (MnO_2) nanosheets can be oriented into planar networked sheets and are economical, biocompatible, and degradable via glutathione[22]. MnO_2 offers efficient fluorescence quenching to further encourage its union with biomolecular imaging probes. Li

et al. showed that MnO_2 can sustain nucleic acid stability and signal amplification with either HCR or CHA as the signal amplifier[23,24]. In both cases, the nucleobases on the probe strands strongly bind to the sheets via physisorption. Without the sheets, there was weak fluorescent output *in vitro.* However, their same probes at identical concentrations generated bright and apparent fluorescence after nanosheet-mediated delivery (Figure 4D).

Other strategies have reported heightened stability. These include the incorporation of secondary structures that promote endonuclease resistence[25] or pH-activatable structures[26] (Table 1). In general, these approaches utilize clever strategies in structural DNA nanotechnology such as structural architectures and pH sensitivity based on C-G base-pair density to avoid interactions with the surrounding microenvironment. However, many purely DNA-based probe structures—whether more stable against endonucleases[25] or more reactive for a decreased fluorescence time[15]—require lipofectamine—a cationic and highly toxic delivery agent[76,77]—to aid in their transfection into cells. While lipofectamine is canonically used as a transfection agent for gene therapy research, its union with HCR and CHA raises safety concerns for *in vivo* imaging. Therefore, the design of probe structures that can be functionalized with a safe helper vehicle—such as targeting ligands or the MnO_2 sheets described above—should be considered more seriously.

In general, many approaches have tackled live cell imaging-related challenges that afflict HCR and CHA (Table 1). Of course, these methods needed to confirm that the probe maintains target specificity. Benchtop selectivity tests—where HCR and CHA probes are mixed with strands besides the target—are commonly implemented to demonstrate the probes' power to discriminate targets from nonspecific binding. Other reports have confirmed selectivity by imaging with probes in cancerous cell cultures in parallel with noncancerous, target-negative cultures[24]. Future *in vitro* specificity experiments can implicate HCR and CHA probes in co-cultured, multidimensional models[64,65] so that the probes can realistically (1) discriminate between healthy and diseased cell lines and (2) map dynamic nucleic acid expressions that both differ and agree between healthy and disease cell lines. These are reasonable precursor experiments to support possible *in vivo* specificity.

Lowering Limit of Detection

The prevalence and lifetime of many nucleic acids can be influenced by a combination of subjective factors such as sex, body weight, and age[27], so a limit of detection (LoD) below femtomolar levels is a paramount goal for strand amplification's clinical translatability[29]. While HCR and CHA have shown novel nucleic acid imaging capabilities, the detection limit for most imaging probes is in the picomolar to femtomolar range (Table 1, Figure 11). Therefore, other strategies on strand amplification employment have been developed for even lower LoD values. Only recently, attomolar to sub-attomolar ranged detection by HCR and CHA has been consistently achieved.

Electrochemical Sensing

Perhaps one of the more successful approaches in lowered LoD is electrochemical sensing. Subtle hybridization events, strand conformational changes, or nucleic acid harnessing of other chemicals through intercalation or physisorption produce slight yet definite redox

changes on the electrode surface for a quantifiable signal[30,31]. The simplicity and lower cost of electrochemical sensors have made them more attractive for DNA detection above PCR, surface-enhanced Raman scattering (SERS) and localized surface plasmon resonance (LSPR). Most electrodes for DNA detection utilize gold because they can easily hybridize with thiolated DNA. Indeed, DNA electrochemical sensors are not new in the biosensor world and already offer attomolar detection[32], but these assay designs require a denser number of input strands for the subsequent readout and can therefore be more costly and time-consuming to prepare. Therefore, strand amplification offers a more efficient and economical way to produce electrochemical nucleic acid sensors.

An increasingly popular strategy in HCR electrochemical sensing involves capturing chemical labels upon hybridization. In particular, derivatives of cationic RuHex $[Ru(NH_3)_6]^{3+}$ have strong affinity to DNA duplexes by electrostatic anchorage on the phosphate backbones. Their accumulation on the strands can generate an oxidation current[33] as the electrochemical reporter of DNA hybridization. Guo et al. utilized this mechanism to sense exosomal miRNA (miR-122) by HCR[34]. Hairpin probes complimentary to the target miRNA were first grafted to a gold electrode surface. Upon hybridization with the target, the rest of the probe hybridizes with the remaining hairpins to catalyze HCR and capture RuHex molecules in an increasingly dense manner (Figure 5A). This method achieved a low LoD of 53 aM and further reduced the chances of false positive signals by introducing exonucleases to the system prior to the start of HCR; probes not conformed into hairpins were digested by the exonucleases and were eliminated from the total output signal. The conformational sensitivity of unhybridized probe strands is important because any slight microenvironmental charge change can result in undesired self-folding and strand collapse, thus accidentally capturing RuHex. Therefore, the endonucleases act as a novel quality control by destroying unbound strands altogether. Lv et al. also studied RuHex captivation by sandwiching the target DNA (*h. pylori* DNA) and HCR event between a gold electrode and gold nanoparticles functionalized with the HCR initiator[35]. The growing HCR concatemers on the nanoparticle surface facilitated an accumulation of dendritic RuHex species on the surface and electrode, thereby resulting in heightened signal. This work achieved an impressive LoD of 0.63 aM.

Immobilization of higher order DNA structures on electrodes can also gather distinguished signals after strand amplification. For example, DNA tetrahedrons were grafted onto gold electrodes with an exposed hairpin probe for the target to catalyze HCR[36] (Figure 5B). The primary role of the tetrahedral motif is to maintain probe stability on the electrode by evading inter-probe entanglement and nonspecific adsorption of other molecules and random strands. This approach resulted in a LoD of 0.93 aM. Another strategy utilized nonlinear, Y-shaped DNA motifs that continuously branch into HCR dendrimers while remaining grafted to the gold electrode[37]. The Y shaped motif was chosen for its stability and heightened selectivity to miR-25 over normal ssDNA and duplex motifs. The purely-DNA based approach led to a higher LoD of 334 aM because no chemical reporters were involved.

Electrochemiluminescence (ECL)

Electrochemiluminescence (ECL) is another signaling approach with low-attomolar LoD. Similar to electrochemical sensors, ECL relies on the change of electron transfer near an electrode surface, but it uniquely generates an excitation state that permits light emission for observable signal[38]. Due to its low background and high sensitivity, ECL has become increasingly attractive in biomolecular sensing applications and is already commonly employed in standard bioanalysis methods such as western blotting and immunoassays. Thus, ECL-based HCR and CHA could bring them closer to more practical biosensor technologies.

For example, Zhang et al. exploited ECL for a 18.6 aM LoD by hybridizing hairpins on ZnO-coated gold nanoparticles such that HCR dendrimers allowed branched electroactive ferrocene[39]. The growing ferrocene density would ultimately consume O_2 coreactants from the ZnO shell, quenching ambient ECL in the sensor. Despite the low LoD, this working mechanism depends on a switched “ON to OFF-state” where the ECL signal is omnipresent only until the target is detected. Ge et al. similarly used HCR-ECL but with desirable “OFF to ON-state” for a 4.97 aM LoD[40]. In their approach, HCR probes are grafted onto mesoporous silica nanoparticles where $AgNO_3$ was loaded inside. $AgNO_3$ was released upon hybridization between the DNA and target RNA strands allowing Ag ions to be captured within cytosine-rich DNA strands that cluster and quench the surrounding quantum dots for heightened ECL.

Magnetic detection strategies

Magnetic signal methods have also achieved impressive attomolar to sub-attomolar LoD (Table 2). For example, bio-bar-coding—first established by Chad Mirkin’s lab[78]—was recently coupled with CHA by Xueji Zhang’s group fora 97.9 zeptomolar LoD of miR-21[41]. This is the lowest established LoD reported using strand signal amplification and enhances traditional bio-bar-coding’s initially reported LoD of 500 zM[78]. Bio-bar-coding operates by sandwiching the target strand between (1) probe gold nanoparticles and (2) magnetic microparticles. Both particle species are functionalized with oligonucleotides such that the target partially hybridizes each of them simultaneously. When the target strand enables dimerization between the gold and magnetic nanoparticles, the gold nanoparticles are magnetically isolated for analysis. Conventionally, the barcode strands would be interpreted alone as amplifiers but Zhang’s group strengthens this process by coupling the barcode strands with CHA after magnetic separation (Figure 6). Additionally, Tang et al demonstrated 13 aM LoD via colorimetric-based detection. They engineered HCR to enable triggered aggregation of magnetic networks, therefore providing an observable colorimetric change in solution[57].

Multiplexed sensing

Nucleic acid molecules have promise as disease biomarkers but can also be non-specific[79]. The simultaneous detection of multiple disease-correlated targets can further validate the extent and presence of diseases. Recent endeavors in strand amplification have therefore explored optimized techniques that enable multiplexity. An earlier work in HCR

demonstrated 5-species multiplexity via five different HCR probe species[9,12]. Progress has since improved multiplexity by maximizing the bandwidth of HCR and CHA probes to recognize multiple targets at once or with minimal probe diversity. Advancements in multiplexed strand amplification have been translated to both imaging and chemical sensing modalities.

Branched and nonlinear DNA nanostructures

One such approach could involve secondary DNA structures that enable probing of multiple targets. Xu et al. designed DNA structures such that traditional HCR hairpin probes are instead designed as branched DNA structures upon hybridization[42]; the probe ultimately cascades into networked DNA superstructures when both target sequences are recognized. However, if only one of the two targets is detected by the probe, then linear and characteristic structures are formed. This is primarily due to the extension of one versus two unique branch sequences for superstructure formation. This method therefore makes it easy to differentiate a product where both targets are present from a product where only one or no targets are present. This approach only needs two probe strands for two targets while traditional HCR would require 4 probe strands. (Figure 7A, B). This work demonstrated multi-sensing of two targets but suggests there is room to engineer the probe for three or even more targets. Lv et al. similarly explored higher order structures using 3D tetrahedron HCR probes[84]. The tetrahedron vertices were functionalized with Y-shaped DNA motifs which possess the necessary HCR hairpins. The Y-shaped motifs were comprised of two different species, allowing the tetrahedron to sense two different target strands within two sites on the total structure (Figure 8A). This work displayed simultaneous imaging of miR-21 and miRNA-203 within the same cells on the same probe by functionalizing them with two different dye-quencher pairs (Cy3-BHQ2 and FAM-BHQ1) for FRET. The different dye-quencher pairs led to resultant red and green fluorescence, making it easy to visually distinguish between the different target species. The resulting micrographs corroborated the different densities of both targets within HeLa and MCF-10A cells (Figure 8B).

Another nonlinear DNA-based method utilized “multiplexed error robust fluorescence *in situ* hybridization” (MERFISH) with branched HCR for multiplexed RNA imaging (Figure 7C)[43]. MERFISH was invented by the same team, Xiaowei Zhuang’s group in 2015,[44] but has since been coupled with HCR in 2019. In principle, MERFISH requires the use of both (1) “error-robust” barcode DNA probes and (2) FISH fluorescent DNA probes for signal upon hybridization. MERFISH has alone measured 140 species of RNA[44]. Above traditional FISH-mediated HCR, MERFISH-HCR achieves impressive brightness because fluorescence from a single target RNA is produced by binding several labeled probes. A weakness to this demonstration, however, is the need for 16 probes per RNA species, which is not practical for *in vivo* applications and may be taxing for biosensor designs. Nonetheless, the significant advancement from 92 required probes to only 16 encourage further work to utilize MERFISH while continuing to minimize diverse barcode probes per target.

Optically-responsive multiplexity

A simple yet efficient demonstration of optically-mediated multiplexity utilized traditional HCR probes with unique time-gated FRET (TG-FRET)[45]. Guo et al. executed this concept by engineering two HCR probe species (based on the two different targets) resulting in two characteristic photoluminescence decay times by installing different TG-FRET molecules within the HCR products. This work demonstrated multiplexing of two miRNAs, but this platform may accommodate higher order multiplexing based on a higher number of allowed relaxation times.

Other optical multiplexing approaches rely on grafting different hairpin probes on nanomaterials with tuned optical responses. For example, Zhao's group immobilized three HCR species and CY3-labeled HCR amplifiers on different 200nm silica photonic crystals (PhCs) (Figure 8C-D)[46]. The PhCs are tuned to reflect characteristic wavelengths of red, green, and blue light. This method is advantageous over naked fluorophore signaling due to PhCs' narrower spectral width, biostability, and reduced background[91]. Meanwhile, the CY3-tagged HCR strands on the PhC surface will accurately correlate fluorescence with target concentration. Upon recognition of the target and consequential HCR cascading, (1) PhC fluorescence will emit and remain relative to target strand concentration, and (2) the surface of the related PhC will reduce scattering and thus change the reflective intensity of the tuned color. The fluorescence and reflectivity of the green, blue, and red particles were compared between each other based on presence of miR-21, miR-155, and miR-210 respectively. As the wavelength difference is maximized between red, green, and blue peaks, this mechanism can only accommodate third-order multiplexity while maintaining distinguishable signals. While this generates a beautiful method to visualize the presence of different miRNAs, it cannot be used for imaging but is rather a photonic biosensor. A similar strategy involved the union between CHA and fluorescent and color-coded microspheres[47]. While the work demonstrated the ability to efficiently sense miR-21, miR-222, and miR-122 at once, the authors claim their platform theoretically allows "as many as 500 targets" to be detected simultaneously.

Clinical Translatability

As explored above, a variety of technical advances have bolstered the strand amplification's viability for clinical analysis. Therefore, more recent reports have deployed HCR and CHA for *in vivo* imaging and proof-of-concept liquid biopsies (either from tissue, blood, or urine samples).

In vivo imaging

HCR-mediated imaging in living organisms has only been demonstrated twice in the last year, yet the platform shows promise for future *in vivo* mapping. The advantages include exploitation of higher order DNA structures for the HCR scaffold and the use of MnO_2 carriers for effective delivery and contrast with the HCR probes.

Wu et al.[48] successfully achieved targeted delivery to cancerous cells so that the HCR probes could correctly and spatially signal the presence of cancerous miR-21. The HCR probe was

only one component of their Y-shaped structural design; two ends of the Y-motif enabled linear HCR while the third end of the Y was covalently conjugated to folic acid, a popular cancer targeting ligand in nanomedical drug delivery systems[80,81] (Figure 9A-B). This work successfully sensed miR-21 in both HeLa and MCF-7 xenografted mice within a span of two hours (Figure 9C), and no lipofectamine reagents were required to aid in the cellular uptake of the probes. Reported LoD was found to be 800fM.

Only several months later, Wei et al. demonstrated HCR-mediated miRNA imaging *in vivo* by combining HCR with magnetic resonance imaging (MRI)[49]. "Honeycomb MnO_2 nanosponges" (hMN) carried the necessary DNA probes to cells and then dissolved into Mn^{2+} ions by glutathione. The HCR probes were coupled with DNAzymes that harness the dissolved Mn^{2+} ions for a magnetic resonance. The growing HCR strands produced an increased collection of Mn^{2+}, resultantly providing a stronger MRI signal. While MRI has notoriously suffered with weak sensitivity and poor contrast as a current live imaging medium, the Mn ions used here enhance the contrast on the localized tumor site, serving as an effective signal amplifier.

Human sample testing

Such recent advances in HCR and CHA-mediated detection have galvanized their ability to sense cfDNA in urine, serum, whole blood, lung fluid, and harvested tissue. These approaches do not use imaging methods but instead advantage from electrochemistry, ECL, optical signaling and even other techniques not previously described. These amplification methods have detected miRNA, ctDNA, tDNA, and enzymatic activity. Other works have reported the detection of these targets when they were artificially spiked in human samples[37,59], i.e., samples from a healthy donor, but these reports will not be detailed here. Here we highlight reports that used clinical samples from patients diagnosed with the disease of interest.

In one example, Zhao used the multiplexed photonic crystals[46] (Figure 8C-D) to detect miR133a, miR-143a, and miR-200b within the serum samples of bladder cancer patients[50]. Jirakova et al. (Table 3) used a multiplexed HCR electrochemical sensor[51] to screen miR-21, let-7a and miR-31 from cervical samples of HSIL alongside samples from healthy women; all healthy samples resulted in near negligible signal while let-7a, miR-21 led to significant signal difference ($p<0.05$). Huang et al. (Table 4) developed an HCR-based electrochemical sensor where two dumbbell-shaped HCR probes self-assemble into nest-like superstructures that only attach to a gold electrode upon hybridization with target circulating tumor DNA (ctDNA)[52]. While the LoD was only 3 pM, this work successfully detected ctDNA in serum and pleural effusion samples from breast cancer and hepatocellular carcinoma patients, respectively. This was also tested against samples from healthy patients, emphasizing the platform's powerful specificity. Their device maintained minimal to low signal in all 24 healthy samples while having heightened electrochemical signal in six of the 23 breast cancer serum samples and two of the 25 pleural effusion hepatocellular carcinoma patients. Urine samples were also screened for telomeric DNA by characterizing HCR-induced gold nanoparticle aggregation networks via dynamic light scattering[63] for the diagnosis of bladder cancer. Their work showed a near 2-fold size increase of aggregates in bladder

cancer urine, while the urine samples from healthy individuals, or individuals with liver, gastric, lung, or prostatic cancer maintained dimensions similar to the non-aggregated control sample.

While this compelling progress invites more exploration on HCR and CHA-based methods for clinical screening, we note that only three recent reports validate selectivity by testing samples from patients versus healthy controls (Table 4). Many other demonstrations validate selectivity only by replacing target strands with mismatched or scrambled sequences against the sensors in buffer. The most powerful assertion of specificity and therefore sensor efficacy would involve the analysis of other human samples where the target is predicted to be absent or significantly less abundant.

Theranostic demonstrations

HCR and CHA also have value for sensing-therapeutic dualities. Besides detection and imaging, some work in strand amplification has established the co-delivery of a drug or therapeutic biomolecule once the target is detected. The ability to intercalate drug molecules within DNA strands or decorate DNA structures with therapeutic strands such as siRNA for gene knockdown suggests that HCR and CHA have theranostic capacity.

For example, Ma et al. described pH-activated HCR[26] and included a delivery modality of antisense oligonucleotides. In their design, the antisense strand was complimentary to miR-21 and was installed at the end of an HCR hairpin (Figure 10). Exposure of this strand to the target miR-21 resulted in a gene silencing efficiency of up to 40%. Wang et al.'s worked on the tetrahedrally-scaffolded HCR for increased reaction rate with a drug release feature for photodynamic therapy. By intercalating methylene blue within the scaffold duplexes, the tetrahedrons could destroy over 70% of the cultured cancer cells upon 650 nm light irradiation within three minutes. This work validated a viable "sense and treat" mechanism by demonstrating sustained FRET signaling of the mi-21 with maximum loading of methylene blue.

While these reports demonstrate a novel new feature to strand-induced signal amplification, their work stopped at *in vitro* demonstrations. The above-mentioned *in vivo* imaging strategies required multivalent HCR probes for cell targeting or stable delivery endeavors, and thus future work on therapeutic duality should investigate if the therapeutic feature might overload the system potentially dampening either the delivery, sensing, or drug release efficiency as opposed to those results found *in vitro.* Additionally, the continued monitoring of HCR sensing signal with respect to release of the drug molecule may more explicitly demonstrate the "sense and treat" duality because both reports depended on viability assays to verify therapeutic efficacy.

Future Outlook

The past two years have demonstrated impressive progress in strand-mediated signal amplification: the field is currently tapping into *in vivo* imaging for the first time, and more work on analyte detection within clinical samples is being reported.

Nucleic acids have been consistently proposed as prognostic biomarkers just as much as diagnostic biomarkers, so future work invites HCR and CHA-related projects to include accurate oversight of target abundance in (1) early or pre-disease states, (2) later disease progression such as during metastasis, and (3) disease abatement alongside ongoing treatment such as chemotherapy, radiation, or immunotherapy. This can validate HCR and CHA's ability to spatially correlate the presence of nucleic acid markers with disease progression.

3D DNA nanostructure probes have consistently improved imaging contrast, reaction time, delivery, complexity in multiplexity, stability in electrochemical sensing as well as intercalation of therapeutic agents for therapeutic duality. This pattern welcomes future research to investigate the use of these 3D DNA nanostructures under *in vivo* imaging applications; this is a particularly motivating avenue to explore as DNA nanotetrahedrons have characteristically increased cellular uptake due to their stable geometry[82]. To date, no 3D motifs have been implemented for *in vivo* HCR or CHA imaging, but this added dimensionality may complement the past report on targeting and sensing *in vivo* with controlled drug release.

Figure 11 shows that electrochemical sensing and ECL have demonstrated the lowest LoD along with the newly emerging bio-ba-coding method. Because these approaches are gaining promise as viable sensors of low-abundant analytes, future research may consider their design and manufacturing from a commercial and economic perspective. Inexpensive materials, coatings, and synthesis processes should be explored more seriously in future research involving these sensor technologies. Future work should also continue to develop the simplest detection approaches that require minimal auxiliary steps, such as washing away of unbound probes, further extraction or isolation of nucleic acids from clinical samples before screening.

The microenvironment within different human samples should also be respected during the probe design process. Provided nucleic acid's susceptibility to unintended conformational changes from pH or electrolytic gradients or its binding abilities with a wide range of proteins[92,93], Guanine-rich probes should be avoided, but nonetheless carefully investigated. For example, potassium-rich environments or other surrounding proteins may cause the spontaneous formation of G-quadruplex motifs, which can in turn collapse amplification probes and obstruct hybridization growth[60]. Strategies to avoid inadvertent secondary structures should be carefully outlined in the context of clinical sample composition. For example, the salt content in urine may give a higher rise to these structural changes while heightened enzymatic activity and diversity in saliva may create a punishing environment for nucleic acid probes.

HCR has made significant contributions towards live cell imaging with a low LoD, good multiplexity, as well as theranostic and clinical translatability. Regardless, DNA signal amplifiers are generally comprised of a wide class of TMSD techniques that have also made novel contributions in this light. Enzyme-free DNA walkers, for example, have been engineered to have activated "walking" modalities upon target miRNA recognition; this resulted in impressive and amplified FRET-based signaling[100]. While hairpin-free entropy

driven catalysis (EDC) has also shown interesting sensor capabilities[110], its reaction speed is slower than CHA and HCR[106], requires more rigorous gel-based purification for stoichiometric accuracy[105], has an LoD in the picomolar range for sensors[107,108,113], and requires whole-blood spiking to achieve effective readouts of target miRNA[109]. While these sub amplification techniques are less robust than HCR and CHA, future research still encourages design optimization strategies that strengthen their translatability and versatility to imaging and detection modalities; diversifying approaches and capabilities within TMSD will widen the trajectory of strand amplification's impact on nucleic acid and molecular-scale diagnostic tools.

While discussed in detail in the live-cell imaging advances, it is noticeable that strand amplification can also detect other target molecules besides nucleic acid in other sensing platforms. For example, CHA was applied to exclusively sense exonuclease 1 for the start of the signal amplification within an electrochemical-based sensor[96]. CHA has also been utilized for the detection of biomarker proteins such as Mucin 1 via electrochemical signaling[111]. While further work is needed to integrate strand amplification electrochemical sensor methods with different target molecules and species, future research will likely involve a more specific comparison of strand amplification's ability to compete with other electrochemical sensors that are engineered to sense proteins, enzymes, and peptides.

Furthermore, imaging modalities beyond fluorescence should be considered in conjunction with HCR and CHA. While fluorescence imaging has provided unrivaled ability to image hybridization events with excellent resolution, it is not a practical imaging modality for *in vivo* applications. Ultrasound, PET, and CT -mediated imaging have already become highly standardized as clinical imaging approaches; coupling HCR and CHA methods with these methods may make them even more applicable for clinical imaging of nucleic acids. While the clinically relevant modalities fall short of fluorescence in terms of resolution and tissue differentiation, they may nonetheless provide sufficient spatial information on the density and distribution of disease-correlated nucleic acid across different regions in the body.

Conclusions

The elegant self-assembly of duplexed DNA strands without enzymatic or thermal intervention has revolutionized nucleic acid sensors. Recent milestones in the sub-disciplines of HCR and CHA for improved nucleic acid detection have advanced their candidacy for clinical translation. Over the last ten to fifteen years, both sub-techniques have made remarkable progress in improving imaging within live cells—ultimately leading to *in vivo* imaging—as well as in lowering LoD with accurate and even multiplexed sensitivity—now charting legitimate demonstrations in clinical sample screening. Though still young, these recent reports *in vivo* and with clinical samples demonstrate robust sensing abilities. Thus, there is a bright outlook for the integration of strand amplification with the current clinical echelon of nucleic acid detection. These advances underline the fundamental power behind molecular programming for trace detection of biological analytes.

Acknowledgements

This publication was supported by the National Cancer Institute of the National Institutes of Health under the Award Number T32 CA153915 and DP137187-S1. The content is solely the responsibility of the authors and does not necessarily represent the official views of the National Institutes of Health. Graphical abstract and Figure 11 were also constructed via Biorender.com.

References

1. Schwarzenbach H, Hoon DSB and Pantel K, Nat Rev Cancer, 2011,11, 426–437. [PubMed: 21562580]
2. Mandel P & Métais P Les acides nucléiques du plasma sanguin chez I'homme. C. R. Acad. Sci. Paris, 1948, 142, 241–243.
3. Vasioukhin V, Anker P, Maurice P, Lyautey J, Lederrey C and Stroun M, BrJ Haematol, 1994, 86, 774–779. [PubMed: 7918071]
4. Mitchell PS, Parkin RK, Kroh EM, Fritz BR, Wyman SK, Pogosova-Agadjanyan EL, Peterson A, Noteboom J,O'Briant KC, Allen A, Lin DW, Urban N, Drescher CW, Knudsen BS, Stirewalt DL, Gentleman R, Vessella RL, Nelson PS, Martin DB and Tewari M, Proceedings of the National Academy of Sciences, 2008,105,10513–10518.
5. Kamat AA, Baldwin M, Urbauer D, Dang D, Han LY, Godwin A, Karlan BY, Simpson JL, Gershenson DM, Coleman RL, Bischoff FZ and Sood AK, Cancer, 2010,116,1918–1925. [PubMed: 20166213]
6. Dirks RM and Pierce NA, Proceedings of the National Academy of Sciences, 2004,101,15275–15278.
7. Yin P, Choi HMT, Calvert CR and Pierce NA, Nature, 2008, 451, 318–322. [PubMed: 18202654]
8. Peng H, Newbigging AM, Reid MS, Uppal JS, Xu J, Zhang H and Le XC, Anal. Chem, 2020, 92, 292–308. [PubMed: 31693332]
9. Choi HMT, Chang JY, Trinh LA, Padilla JE, Fraser SE and Pierce NA, Nat Biotechnol, 2010, 28,1208–1212. [PubMed: 21037591]
10. Choi HMT, Beck VA and Pierce NA, ACS Nano, 2014, 8, 4284–4294. [PubMed: 24712299]
11. Wu Z, Liu G-Q, Yang X-L and Jiang J-H, J. Am. Chem. Soc, 2015,137, 6829–6836. [PubMed: 25969953]
12. Choi HMT, Schwarzkopf M, Fornace ME, Acharya A, Artavanis G, Stegmaier J, Cunha A and Pierce NA, Development, 2018,145, devl65753
13. Li S, Li P, Ge M, Wang H, Cheng Y, Li G, Huang Q, He H, Cao C, Lin D and Yang L, Nucleic Acids Research, 2020, 48, 2220–2231. [PubMed: 32020194]
14. Huang D-J, Cao T, Huang Z-M, Wu Z, Tang L-J and Jiang J-H, Chem. Commun, 2019, 55, 3899–3902.
15. Wang J, Wang D-X, Ma J-Y, Wang Y-X and Kong D-M, Chem. Sci, 2019,10, 9758–9767. [PubMed: 32055345]
16. Qing Z, Hu J, Xu J, Zou Z, Lei Y, Qing T and Yang R, Chem. Sci, 2020,11,1985–1990.
17. Lakhin AV, Tarantul VZ and Gening LV, Acta Naturae, 2013, 5, 34–43. [PubMed: 24455181]
18. Qin Y, Li D, Yuan R and Xiang Y, Nanoscale, 2019,11,16362–16367. [PubMed: 31435631]
19. 1Chang X, Zhang C, Lv C, Sun Y, Zhang M, Zhao Y, Yang L, Han D and Tan W, J. Am. Chem. Soc, 2019, 141,12738–12743. [PubMed: 31328519]
20. Hahn J, Wickham SFJ, Shih WM and Perrault SD, ACS Nano, 2014, 8, 8765–8775. [PubMed: 25136758]
21. Chu H, Zhao J, Mi Y, Zhao Y and Li L, Angew. Chem. Int. Ed, 2019, 58,14877–14881.
22. Yang K, Zeng M, Fu X, Li J, Ma N and Tao L, RSC Adv., 2015, 5, 104245–104249.
23. Li G, Li J and Li Q, Nanoscale, 2019,11, 20456–20460. [PubMed: 31637399]
24. Li G-L, Xia Y-H and Li Q, Microchemical Journal, 2020,153,104367.
25. Chen J, Yang H-H, Yin W, Zhang Y, Ma Y, Chen D, Xu Y, Liu S-Y, Zhang L, Dai Z and Zou X, Anal. Chem, 2019, 91, 4625–4631. [PubMed: 30856329]

26. Ma W, Chen B, Zou S, Jia R, Cheng H, Huang J, Wang H, He X and Wang K, Anal. Chem, 2019, 91,12538–12545. [PubMed: 31476869]
27. Raffort J, Hinault C, Dumortier O and Van Obberghen E, Diabetologia, 2015, 58,1978–1992. [PubMed: 26155747]
28. Cohen L, Hartman MR, Amardey-Wellington A and Walt DR, Nucleic Acids Research, 2017, 45, el37–el37.
29. Wang J, Yi X, Tang H, Han H, Wu M and Zhou F, Anal. Chem, 2012, 84, 6400–6406. [PubMed: 22788545]
30. Drummond TG, Hill MG and Barton JK, Nat Biotechnol, 2003, 21,1192–1199. [PubMed: 14520405]
31. Paleček E, Fojta M and Jelen F, Bioelectrochemistry, 2002, 56, 85–90. [PubMed: 12009450]
32. Rasheed PA and Sandhyarani N, Analyst, 2015,140, 2713–2718. [PubMed: 25690320]
33. De Rache A, Doneux T, Kejnovská I and Buess-Herman C, Journal of Inorganic Biochemistry, 2013,126, 84–90. [PubMed: 23787142]
34. Guo Q, Yu Y, Zhang H, Cai C and Shen Q, Anal. Chem, 2020, 92, 5302–5310. [PubMed: 32148013]
35. Lv M-M, Fan S-F, Wang Q-L, Lv Q-Y, Song X and Cui H-F, Microchim Acta, 2020,187, 73.
36. Chen X, Huang J, Zhang S, Mo F, Su S, Li Y, Fang L, Deng J, Huang H, Luo Z and Zheng J, ACS Appl. Mater. Interfaces, 2019, 11, 3745–3752. [PubMed: 30624036]
37. Zhou L, Wang Y, Yang C, Xu H, Luo J, Zhang W, Tang X, Yang S, Fu W, Chang K and Chen M, Biosensors and Bioelectronics, 2019,126, 657–663. [PubMed: 30529897]
38. Richter MM, Chem. Rev, 2004,104, 3003–3036. [PubMed: 15186186]
39. Zhang X, Li W, Zhou Y, Chai Y and Yuan R, Biosensors and Bioelectronics, 2019,135, 8–13. [PubMed: 30981028]
40. Ge J, Li C, Zhao Y, Yu X and Jie G, Chem. Commun, 2019, 55, 7350–7353.
41. Tang S, Gu Y, Lu H, Dong H, Zhang K, Dai W, Meng X, Yang F and Zhang X, Analytica Chimica Acta, 2018,1004,1–9. [PubMed: 29329703]
42. Xu G, Lai M, Wilson R, Glidle A, Reboud J and Cooper JM, Microsyst Nanoeng, 2019, 5, 37. [PubMed: 31636927]
43. Xia C, Babcock HP, Moffitt JR and Zhuang X, Sci Rep, 2019, 9, 7721. [PubMed: 31118500]
44. Chen KH, Boettiger AN, Moffitt JR, Wang S and Zhuang X, Science, 2015, 348, aaa6090–aaa6090. [PubMed: 25858977]
45. Guo J, Mingoes C, Qiu X and Hildebrandt N, Anal. Chem, 2019, 91, 3101–3109. [PubMed: 30657312]
46. Zhang D, Bian F, Cai L, Wang T, Kong T and Zhao Y, Biosensors and Bioelectronics, 2019,143,111629. [PubMed: 31470170]
47. Wang J, Sun Y, Lau C and Lu J, Anal Bioanal Chem, 2020, 412, 3019–3027. [PubMed: 32232523]
48. Wu G, Chen T-T, Wang X-N, Ke Y and Jiang J-H, Chem. Sci, 2020,11, 62–69. [PubMed: 32110357]
49. Wei J, Wang H, Wu Q, Gong X, Ma K, Liu X and Wang F, Angew. Chem, 2020,132, 6021–6027.
50. Wei X, Bian F, Cai X, Wang Y, Cai L, Yang J, Zhu Y and Zhao Y,Anal. Chem, 2020, 92, 6121–6127. [PubMed: 32227890]
51. Jirakova L, Hrstka R, Campuzano S, Pingarróon JM and Bartosik M, Electroanalysis, 2019, 31, 293–302.
52. Huang Y, Tao M, Luo S, Zhang Y, Situ B, Ye X, Chen P, Jiang X, Wang Q and Zheng L, Analytica Chimica Acta, 2020, 1107, 40–47. [PubMed: 32200900]
53. Li Y, Yue S, Qi H, Ding C, Song W and Bi S, Chem. Commun, 2019, 55, 4103–4106.
54. Liu G, Chai H, Tang Y and Miao P, Chem. Commun, 2020, 56,1175–1178.
55. Wen X, Yuan B, Zhang J, Meng X, Guo Q, Li L, Li Z, Jiang H and Wang K, Chem. Commun, 2019, 55, 6114–6117.
56. Chang X, Zhang C, Lv C, Sun Y, Zhang M, Zhao Y, Yang L, Han D and Tan W, J. Am. Chem. Soc, 2019, 141, 12738–12743. [PubMed: 31328519]

57. Tang S, Li Y, Zhu A, Yao Y, Sun J, Zheng F, Lin Z and Shen W, Chem. Commun, 2019, 55, 8386–8389.
58. Yu L, He P, Xu Y, Kou X, Yu Z, Xie X and Miao P, Sensors and Actuators B: Chemical, 2020, 313,128015.
59. Feng Q, Wang M, Han X, Chen Q, Dou B and Wang P, ACS Appl. Bio Mater, 2020, 3,1276–1282.
60. Jia L-P, Wang L-J, Ma R-N, Shang L, Zhang W, Xue Q-W and Wang H-S, Talanta, 2018,179, 414–419. [PubMed: 29310253]
61. Ge J, Zhang L-L, Liu S-J, Yu R-Q and Chu X, Anal. Chem, 2014, 86,1808–1815. [PubMed: 24417222]
62. Zhuang W, Li Y, Chen J, Liu W and Huang H, Anal. Methods, 2019,11, 2597–2604.
63. Li T, Zou L, Zhang J, Li G and Ling L, Analytica Chimica Acta, 2019,1065, 90–97. [PubMed: 31005155]
64. Goers L, Freemont P and Polizzi KM, J. R. Soc. Interface, 2014,11, 20140065. [PubMed: 24829281]
65. Swaminathan S, Cranston AN and Clyne AM, Tissue Engineering Part C: Methods, 2019, 25, 609–618. [PubMed: 31441384]
66. Wark AW, Lee HJ and Corn RM, Angew. Chem. Int. Ed, 2008, 47, 644–652.
67. Burnham P, Dadhania D, Heyang M, Chen F, Westblade LF, Suthanthiran M, Lee JR and De Vlaminck I, NatCommun, 2018, 9, 2412.
68. Hyun K-A, Gwak H, Lee J, Kwak B and Jung H.-l., Micromachines, 2018, 9, 340.
69. Stroun M, Anker P, Maurice P, Lyautey J, Lederrey C and Beljanski M, Oncology, 1989, 46, 318–322. [PubMed: 2779946]
70. Liao P-H, Chang Y-C, Huang M-F, Tai K-W and Chou M-Y, Oral Oncology, 2000, 36, 272–276. [PubMed: 10793330]
71. Birkenkamp-Demtröder K, Nordentoft I, Christensen E, Høyer S, Reinert T, Vang S, Borre M, Agerbaek M, Jensen JB, Ørntoft TF and Dyrskjøt L, European Urology, 2016, 70, 75–82. [PubMed: 26803478]
72. Hulbert A, Jusue-Torres I, Stark A, Chen C, Rodgers K, Lee B, Griffin C, Yang A, Huang P, Wrangle J, Belinsky SA, Wang T-H, Yang SC, Baylin SB, Brock MV and Herman JG, Clin Cancer Res, 2017, 23,1998–2005. [PubMed: 27729459]
73. Bronkhorst AJ, Lingerer V and Holdenrieder S, Biomolecular Detection and Quantification, 2019,17,100087. [PubMed: 30923679]
74. Cocucci E, Racchetti G and Meldolesi J, Trends in Cell Biology, 2009,19, 43–51. [PubMed: 19144520]
75. Hu Z, Chen X, Zhao Y, Tian T, Jin G, Shu Y, Chen Y, Xu L, Zen K, Zhang C and Shen H, JCO, 2010, 28,1721–1726.
76. Zhong Y-Q, Wei J, Fu Y-R, Shao J, Liang Y-W, Lin Y-H, Liu J and Zhu Z-H, Nan Fang Yi Ke DaXue Xue Bao, 2008, 28, 1981–1984.
77. Rust A, Hassan HHA, Sedelnikova S, Niranjan D, Hautbergue G, Abbas SA, Partridge L, Rice D, Binz T and Davletov B, Sci Rep, 2015, 5,12444. [PubMed: 26207613]
78. Nam J-M, Stoeva SI and Mirkin CA, J. Am. Chem. Soc, 2004,126, 5932–5933. [PubMed: 15137735]
79. Luck ME, Muljo SA and Collins CB, J.I, 2015, 194, 5047–5052.
80. Zwicke GL, Ali Mansoori G and Jeffery CJ, Nano Reviews, 2012, 3,18496.
81. Fernández M, Javaid F and Chudasama V, Chem. Sci, 2018, 9, 790–810. [PubMed: 29675145]
82. Lee H, Lytton-Jean AKR, Chen Y, Love KT, Park AI, Karagiannis ED, Sehgal A, Querbes W, Zurenko CS, Jayaraman M, Peng CG, Charisse K, Borodovsky A, Manoharan M, Donahoe JS, Truelove J, Nahrendorf M, Langer R and Anderson DG, Nature Nanotech, 2012, 7, 389–393.
83. Cheng H, Li W, Duan S, Peng J, Liu J, Ma W, Wang H, He X and Wang K, Anal. Chem, 2019, 91,10672–10678. [PubMed: 31355629]
84. Lv M-M, Wu Z, Yu R-Q and Jiang J-H, Chem. Commun, 2020, 10.1039.D0CC01626H.
85. Xiong Y, Chen Y, Ding L, Liu X and Ju H, Analyst, 2019,144, 4545–4551. [PubMed: 31268085]

86. Bustin SA and Nolan T, J Biomol Tech, 2004,15,155–166. [PubMed: 15331581]
87. Li Z, Yuan B, Lin X, Meng X, Wen X, Guo Q, Li L, Jiang H and Wang K, Talanta, 2020, 215,120889. [PubMed: 32312435]
88. Kimoto M, Shermane Lim YW and Hirao I, Nucleic Acids Research, 2019, 47, 8362–8374. [PubMed: 31392985]
89. Proudnikov D and Mirzabekov A, Nucleic Acids Res., 1996, 24, 4535–4542. [PubMed: 8948646]
90. Samanta A and Medintz IL, Nanoscale, 2016, 8, 9037–9095. [PubMed: 27080924]
91. Wang Y, Shang L, Bian F, Zhang X, Wang S, Zhou M and Zhao Y, Small, 2019,15,1900056.
92. Herdy B, Mayer C, Varshney D, Marsico G, Murat P, Taylor C, D'Santos C, Tannahill D and Balasubramanian S, Nucleic Acids Research, 2018, 46,11592–11604. [PubMed: 30256975]
93. González V, Guo K, Hurley L and Sun D, J. Biol. Chem, 2009, 284, 23622–23635. [PubMed: 19581307]
94. Zhou H, Liu J, Xu J-J, Zhang S-S and Chen H-Y, Chem. Soc. Rev, 2018, 47,1996–2019 [PubMed: 29446429]
95. Li D, Wu Y, Gan C, Yuan R and Xiang Y, Nanoscale, 2018,10,17623–17628. [PubMed: 30204195]
96. Zhou M, Feng C, Mao D, Yang S, Ren L, Chen G and Zhu X, Biosensors and Bioelectronics, 2019,142,111558. [PubMed: 31387027]
97. Yurke B, Turberfield AJ, Mills AP, Simmel FC and Neumann JL, Nature, 2000, 406, 605–608. [PubMed: 10949296]
98. Green SJ, Lubrich D and Turberfield AJ, Biophysical Journal, 2006, 91, 2966–2975. [PubMed: 16861269]
99. Thakur BK, Zhang H, Becker A, Matei I, Huang Y, Costa-Silva B, Zheng Y, Hoshino A, Brazier H, Xiang J, Williams C, Rodriguez-Barrueco R, Silva JM, Zhang W, Hearn S, Elemento O, Paknejad N, Manova-Todorova K, Welte K, Bromberg J, Peinado H and Lyden D, Cell Res, 2014, 24, 766–769. [PubMed: 24710597]
100. Hu M, Mao D, Liu X, Ren L, Zhou M, Chen X and Zhu X, Theranostics, 2019, 9, 5914–5923. [PubMed: 31534528]
101. He M, He M, Zhang J, Liu C, Pan Q, Yi J and Chen T, Talanta, 2020, 207,120287. [PubMed: 31594575]
102. Karunanayake Mudiyanselage APKK, Yu Q, Leon-Duque MA, Zhao B, Wu R and You M, J. Am. Chem. Soc, 2018, 140, 8739–8745. [PubMed: 29944357]
103. Zhang Z, Fan TW and Hsing l.-M., Nanoscale, 2017, 9, 2748–2754. [PubMed: 28155931]
104. Zhu Z, Tang Y, Jiang YS, Bhadra S, Du Y, Ellington AD and Li B, Sci Rep, 2016, 6, 36605. [PubMed: 27812041]
105. Arter WE, Yusim Y, Peter Q, Taylor CG, Klenerman D, Keyser UF and Knowles TPJ, ACS Nano, 2020,14, 5763–5771. [PubMed: 32293175]
106. Jung C and Ellington AD, Acc. Chem. Res, 2014, 47,1825–1835. [PubMed: 24828239]
107. Shi H, Dai J, Wang F, Xia Y, Xiao D and Zhou C, Anal. Methods, 2020,12, 2779–2784. [PubMed: 32930309]
108. Zhang K, Wang K, Zhu X and Xle M, Analytica Chimica Acta, 2017, 949, 53–58. [PubMed: 27876145]
109. Zhang N, Shi X-M, Guo H-Q, Zhao X-Z, Zhao W-W, Xu J-J and Chen H-Y, Anal. Chem, 2018, 90,11892–11898. [PubMed: 30229657]
110. He L, Lu D, Liang H, Xie S, Zhang X, Liu Q, Yuan Q and Tan W, J. Am. Chem. Soc, 2018,140, 258–263. [PubMed: 29211455]
111. Zhao R-N, Feng Z, Zhao Y-N, Jia L-P, Ma R-N, Zhang W, Shang L, Xue Q-W and Wang H-S, Talanta, 2019, 200, 503–510. [PubMed: 31036215]
112. Dai W, Zhang J, Meng X, He J, Zhang K, Cao Y, Wang D, Dong H and Zhang X, Theranostics, 2018, 8, 2646–2656. [PubMed: 29774065]
113. Meng H-M, Shi X, Chen J, Gao Y, Qu L, Zhang K, Zhang X-B and Li Z, ACS Sens., 2020, 5,103–109. [PubMed: 31903754]

114. Shi H, Wang Y, Zheng J, Ning L, Huang Y, Sheng A, Chen T, Xiang Y, Zhu X and Li G, ACS Nano, 2019,13,12840–12850. [PubMed: 31603651]

115. Raghavendra P and Pullaiah T, in Advances in Cell and Molecular Diagnostics, Elsevier, 2018, pp. 33–55.

116. Wang M, Yu F, Ding H, Wang Y, Li P and Wang K, Molecular Therapy - Nucleic Acids, 2019,16, 791–804. [PubMed: 31163321]

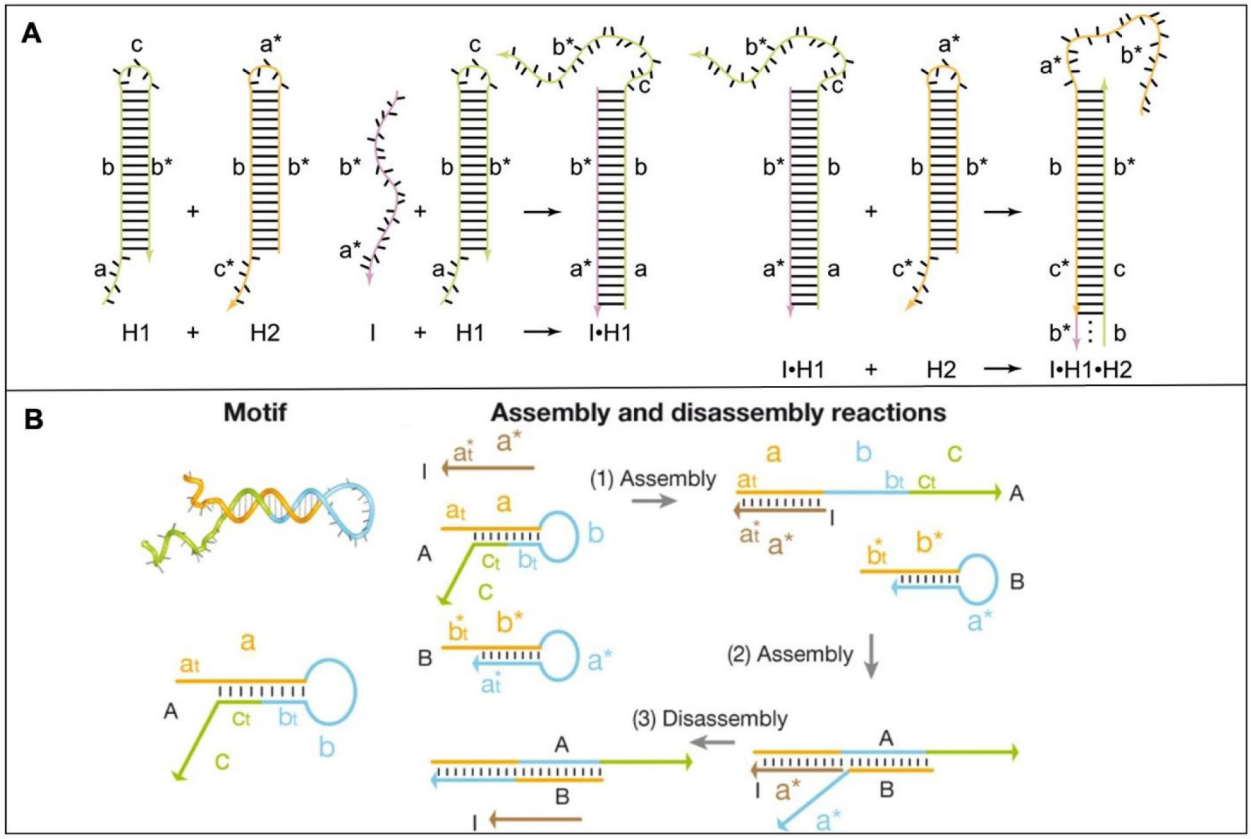

Figure 1:

Strand-hybridization induced signal amplification methods. **(A)** Basic principles of HCR, where the target strand (purple) fuels duplex amplification by hybridizing with loop probe 1 (green), thus exposing the remaining unbound region of probe 1 to hybridize with probe 2 (orange). Copyright (2004) National Academy of Sciences, U.S.A.[6] **(B)** Principles of CHA. Copyright 2008, Nature Publishing Group[7].

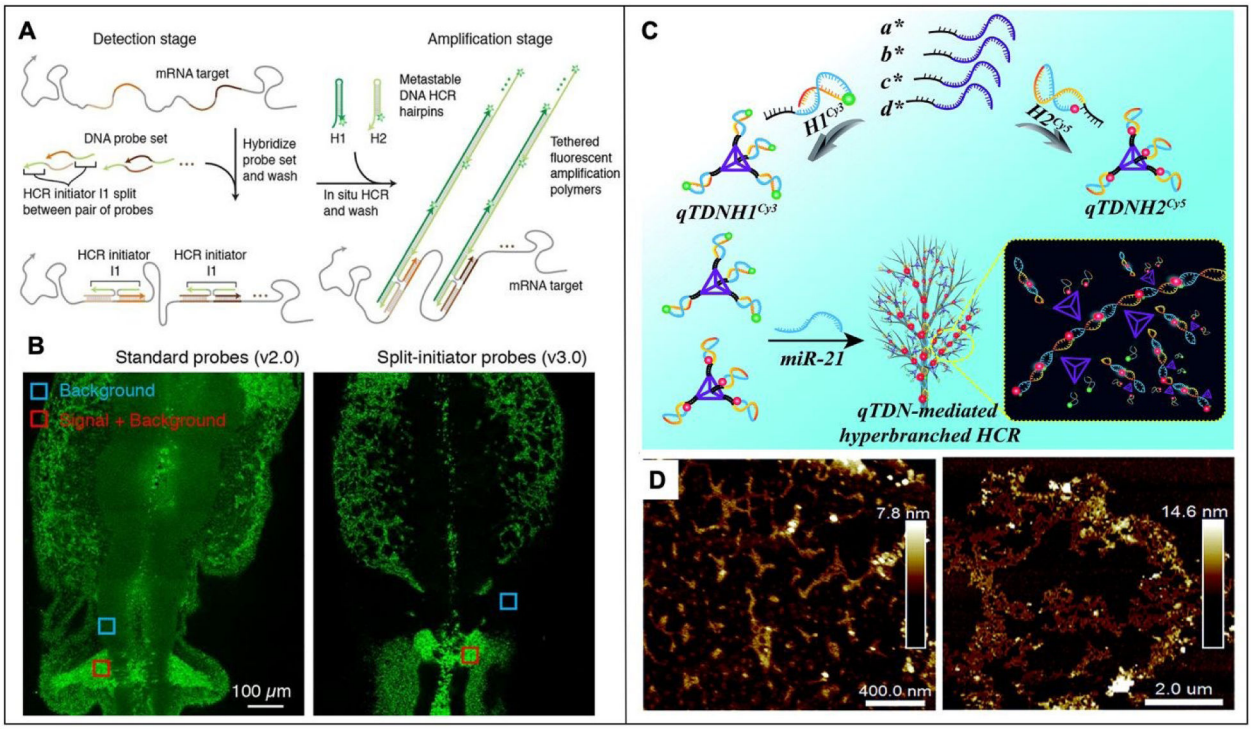

Figure 2:

(A) Schematic on third generation HCR where split initiator probes improve the specificity of the fuel strand binding for an amplified signal. **(B)** Comparison of second-generation HCR with third generation HCR where the background fluorescence in third generation HCR is noticeably minimized with the split initiator probe method. Copyright 2018 Company of Biologists.[12] **(C)** Schematic representation of tetrahedron mediated HCR (qTDNH), which leads to accelerated signal amplification time and larger superstructures based on fuel strand-initiated assembly. **(D)** Generated superstructures using (left) traditional HCR and (right) tetrahedron enabled HCR. Published by the Royal Society of Chemistry 2019.[15]

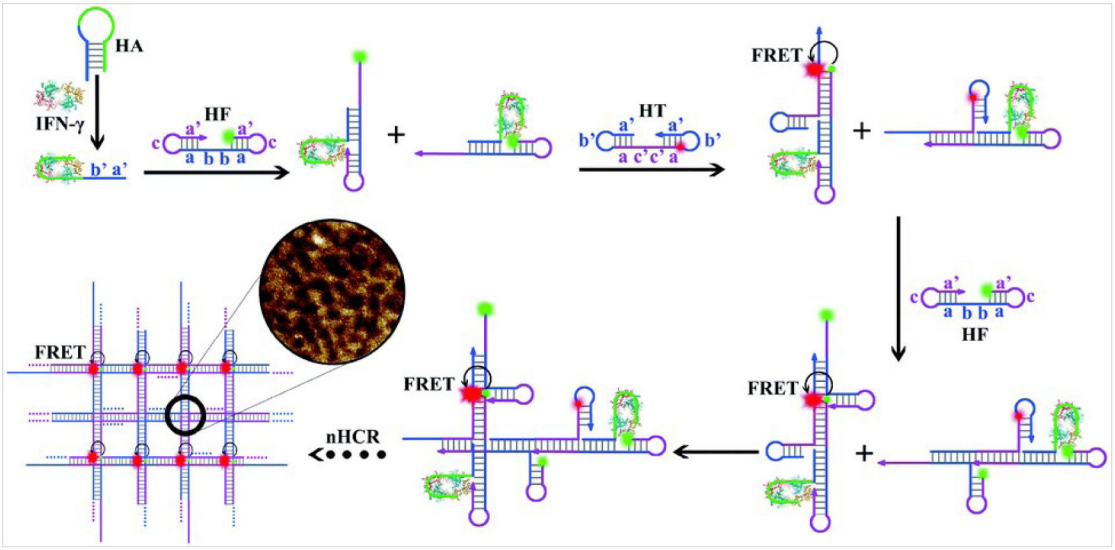

Figure 3:

Aptamer-activated HCR networks for the sensing of I FN-γ whereby the output signal is provided by FRET fluorescence. The multiple conformations adopted after each cascaded hybridization upon incident I FN-γ recognition enables the crosslinked and mesh superstructures. I FN-γ initially binds with hairpin aptamer (HA), which consequently links with fluorescent FAM-dye-labeled and TAMRA-labeled hairpins (HF), (HT) for effective FRET. Copyright 2019 Nanoscale, Royal Society of Chemistry.[18]

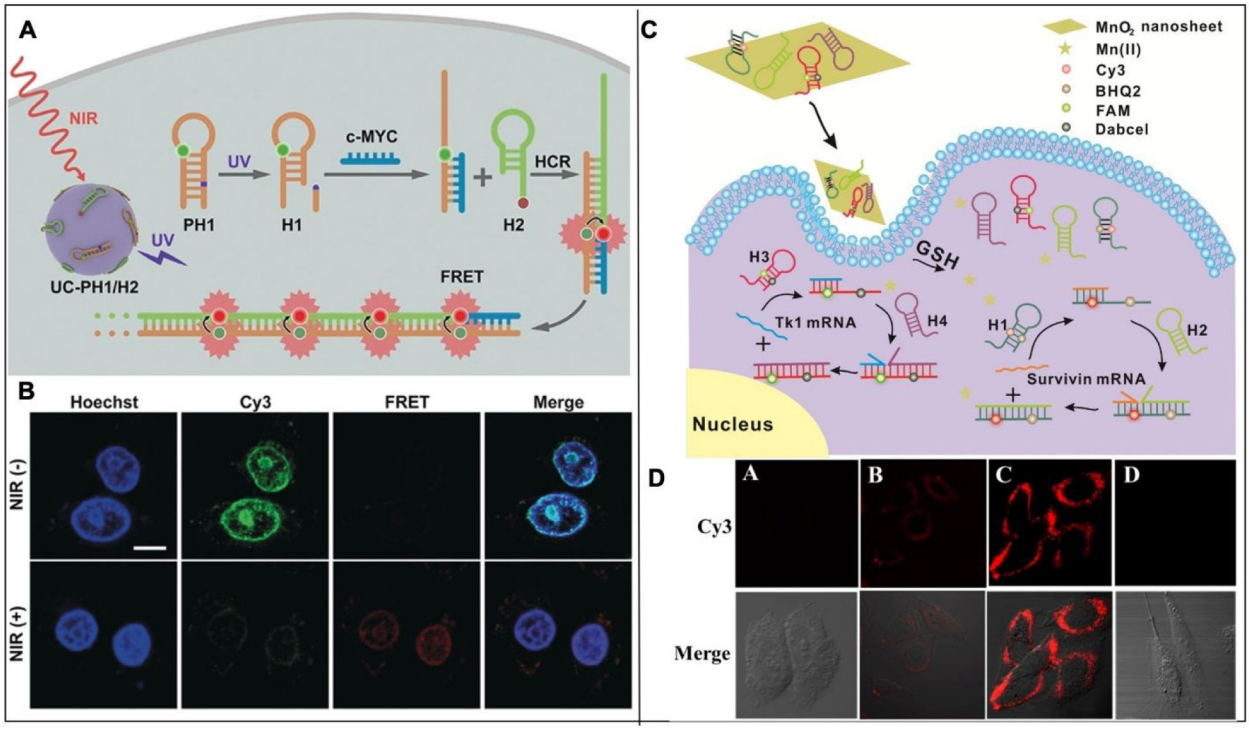

Figure 4:

Sustaining stability and safety when administering HCR and CHA probes to live cells. (A) UCNP mediated HCR allows the HCR probes to remain stable en route to target cells while the NIR activation leads to UV cleaving of the hairpin probes thus preparing them for hybridization with the target and signal amplification. (B) Resulting images of the cells: without NIR activation (above), Cy3 signal dominates while FRET Copyright 2019 Angewandte Chemie International Edition[21]. (C) MnO_2.mediated delivery of CHA signal amplification. **(D)** Validation of MnO_2 delivery efficacy where **Da** depicts the hairpin probes without the sheets, **Db** Hairpin probe **1** with the nanosheet, **Dc** both hairpin probes delivered by the nanosheet, and **Dd** incubated with a cell line that is negative of the target miRNA. Copyright 2019 Microchemical Journal.[24]

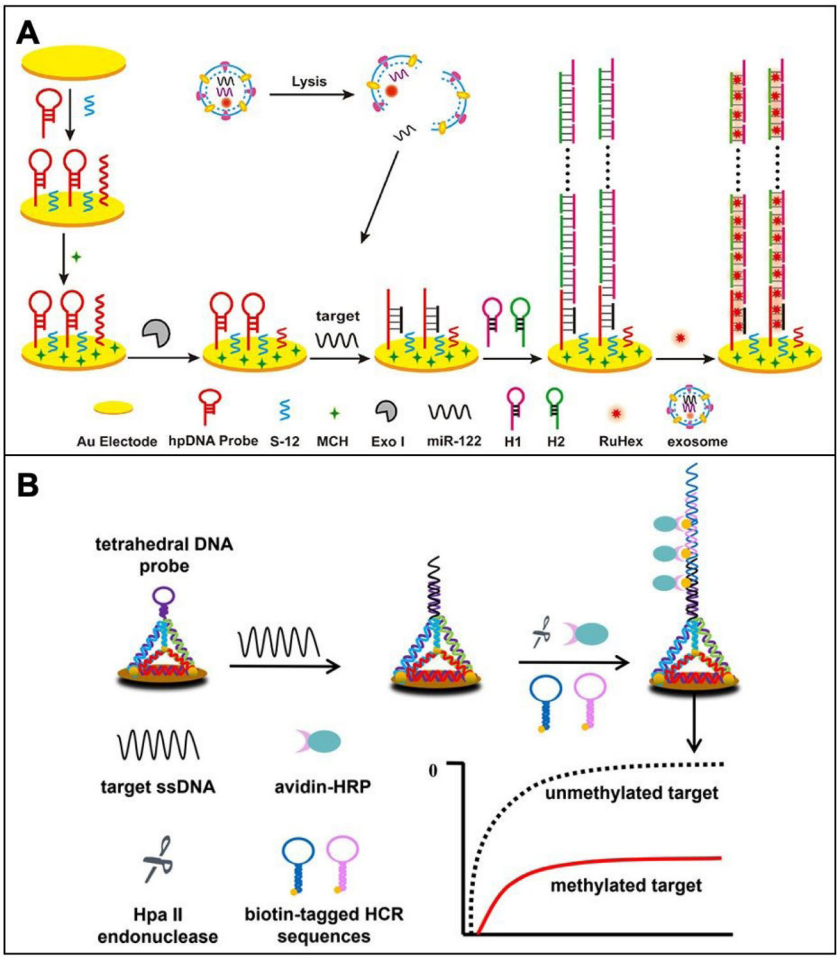

Figure 5.

Electrochemical approaches in lowering the detection limit of target analytes. **(A)** Schematic on RuHex-mediated capture using HCR, where S-2 strands evenly space the HCR hairpin probes and MCH (6-mercapto-1-hexanol) effectively covers bare surface binding sites. Copyright 2020, American Chemical Society.[34] **(B)** Schematic on DNA tetrahedron-mediated electrochemical sensing of methylated DNA. HCR probes are decorated at the point of DNA tetrahedron motifs, which are immobilized on the gold electrode for an even separation of the reduction of both background and nonspecific binding. In this case, HCR probes were decorated with biotin so they could capture avidin-functionalized horseradish peroxidase as a chemical reporter Copyright 2019, American Chemical Society.[36]

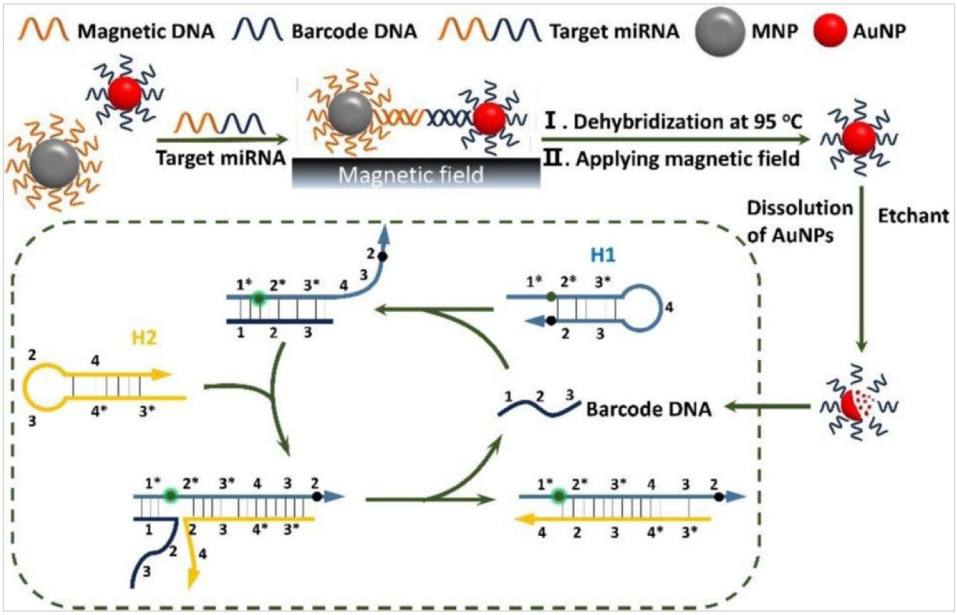

Figure 6.

Schematic on CHA-mediated Bio-Barcoding. CHA is introduced into the Bio-Bar-Coding system after barcoded DNA is isolated from the magnetically-separated gold nanoparticle probes. This achieved 97.9 zM LoD, being the lowest value yet reported. Adapted with permission[41], Elsevier, 2018

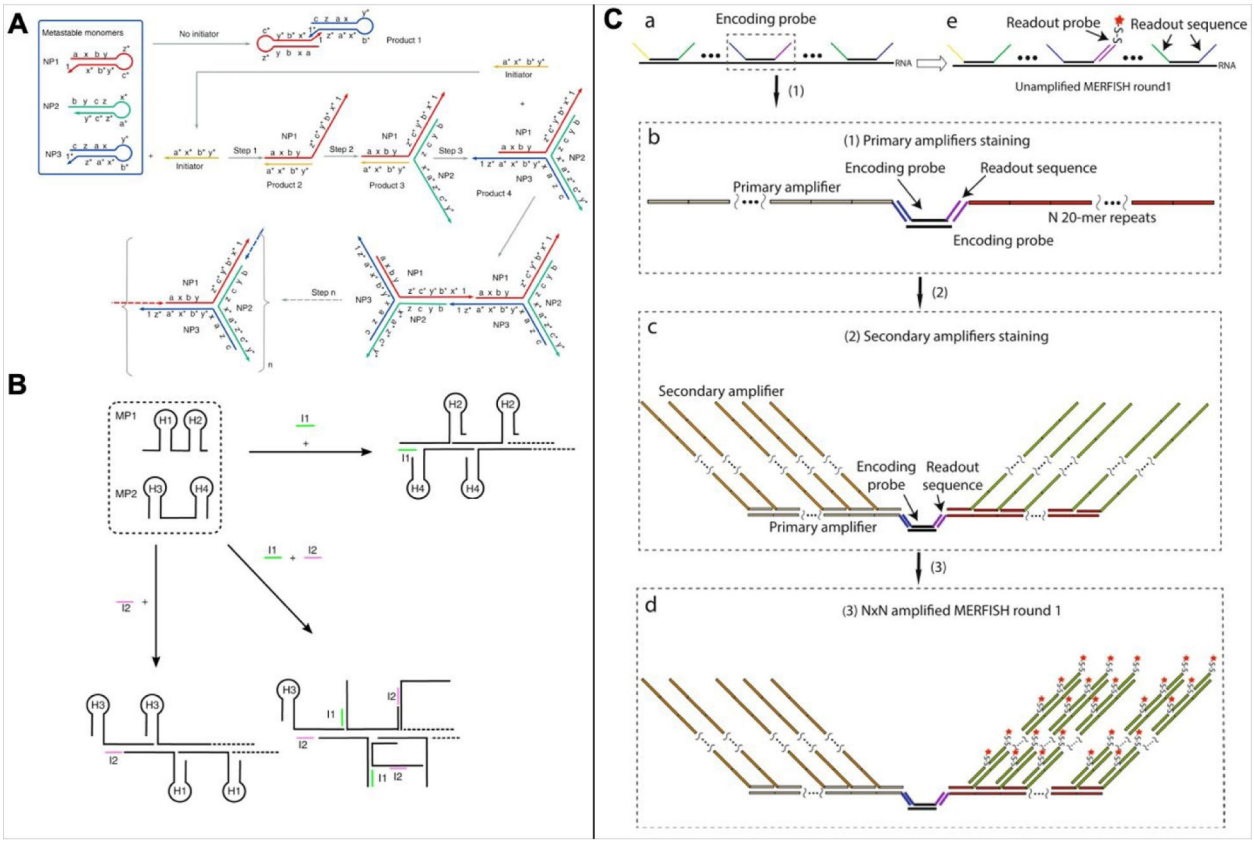

Figure 7.

Strategies in nonlinear and branched HCR for improved multiplexity. **(A)** Schematic of branched HCR amplification method, where the detection of one target leads to serial strand displacement and hyperbranched products. **(B)** Multiplex feature of the branch strategy, where target 1 and 2 (I1 and I2) trigger with hairpins H1-2 and H3-4, respectively. The presence of both targets results in the hierarchical organization of the HCR loop strands. On the other hand, the presence of only one target produces linear, “chain-like” HCR structures, regardless of which target is chosen. Adapted from Microsystems and Nanoengineering, Nature Publishing 2018[42]. http://creativecommons.org/licenses/by/4.0/. **(C)** MERFISH approach. **Ca-b,** the encoding probes which bind to multiple points of the target strand, which simultaneously link to the readout strand. **Cc-d** secondary and then HCR-mediated amplification of the MERFISH sensing. Adapted from Scientific Reports, Nature Publishing 2019[43]. http://creativecommons.org/licenses/by/4.0/

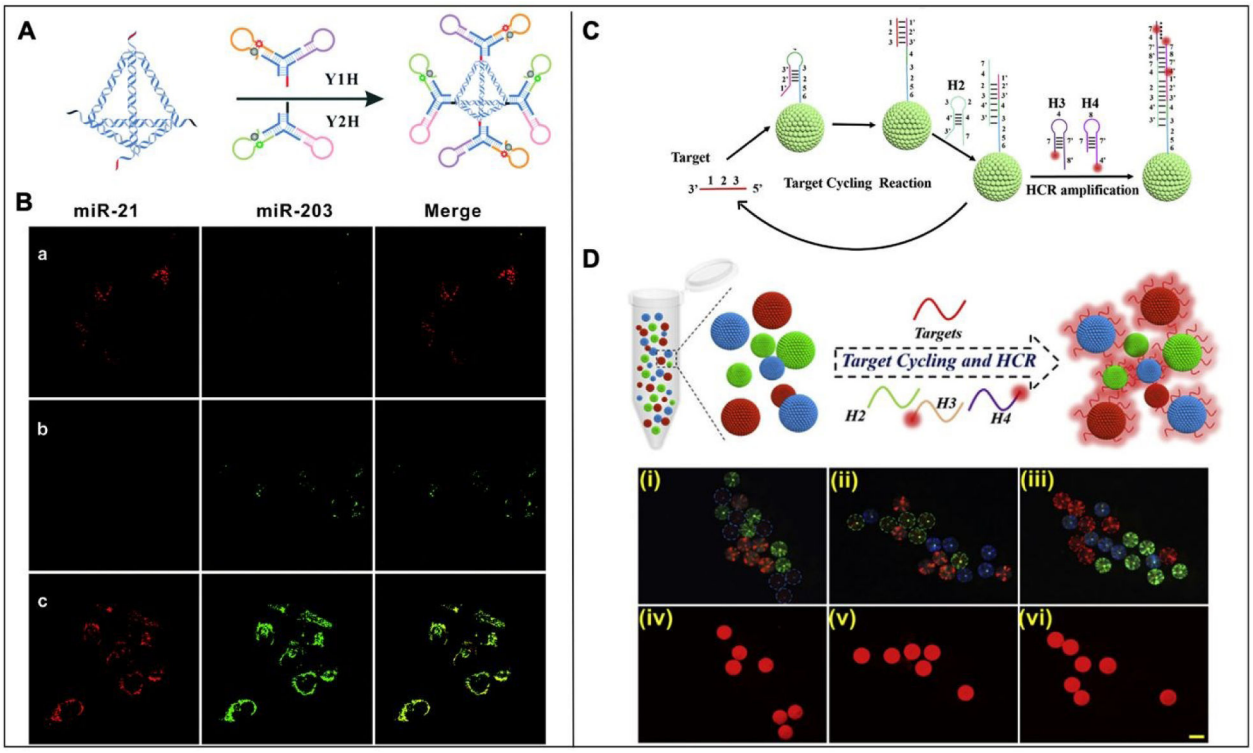

Figure 8:

Strategies in visualized multiplexed strand signal amplification using live cell imaging or biosensors. **(A)** Schematic representation of tetrahedron multiplexed HCR. **(B)** Resultant multiplexed imaging of miR-21 and miR-203 in **Ba** HeLa cells, **Bb** MCF-10A and **Be** HeLa pretreated with miR203. Reproduced from ref 84 with permission from Royal Society of Chemistry. **(C)** Dopamine surface functionalization of photonic crystals (PhCs) to enable attachment of HCR probes on their surface. Probes that recognize three different targets are grafted onto PhCs that are optically tuned to reflect either blue, green, or red reflection peaks as seen in **(D). (D)** (i)-(iii) optical microscopy of the PhCs after recognition of different target nucleic acids, where the intensity of reflected color is diminished with the corresponding PhCs whose HCR reactions are catalyzed. Copyright 2019 Biosensors and Bioelectronics[46]

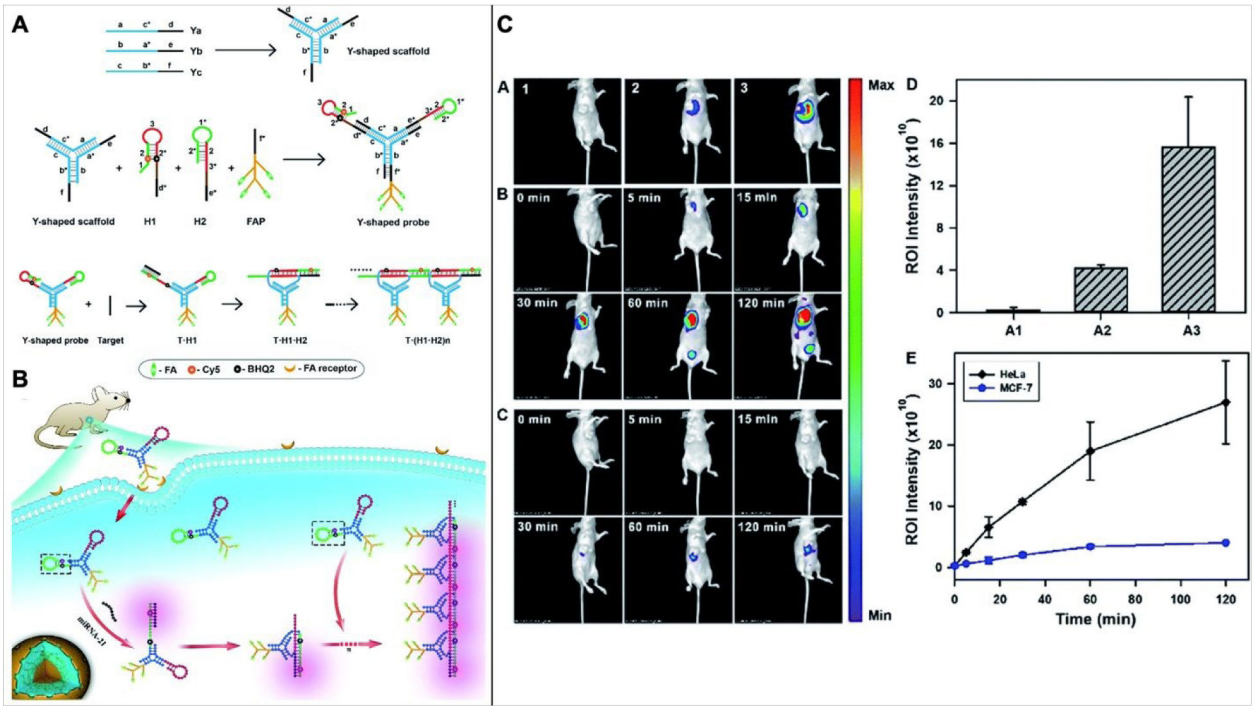

Figure 9.

In vivo imaging in live mice using Y-motif HCR probes. **(A)** Design of a Y-shaped motif where the two top ends are utilized for HCR while the third bottom end is linked with folic acid protein for cancer-cell targeting. **(B)** Schematic of the delivery of Y-HCR probes for cancer cell fluorescent imaging in live mice. **(C)** Fluorescent imaging data of live mice where **Ca** represents mice injected with either saline, MCF-7, or HeLa (from left to right. **Cb** represents HCR fluorescence of the HeLa in the span of 2 hours while **Cc** represents HCR fluorescence of the MCF-7 in the span of 2 hours. **Cd** Consequential fluorescence intensity in region of interest (ROI) and **Ce** Reaction time versus ROI intensity). Copyright 2019, Published by The Royal Society of Chemistry[48].

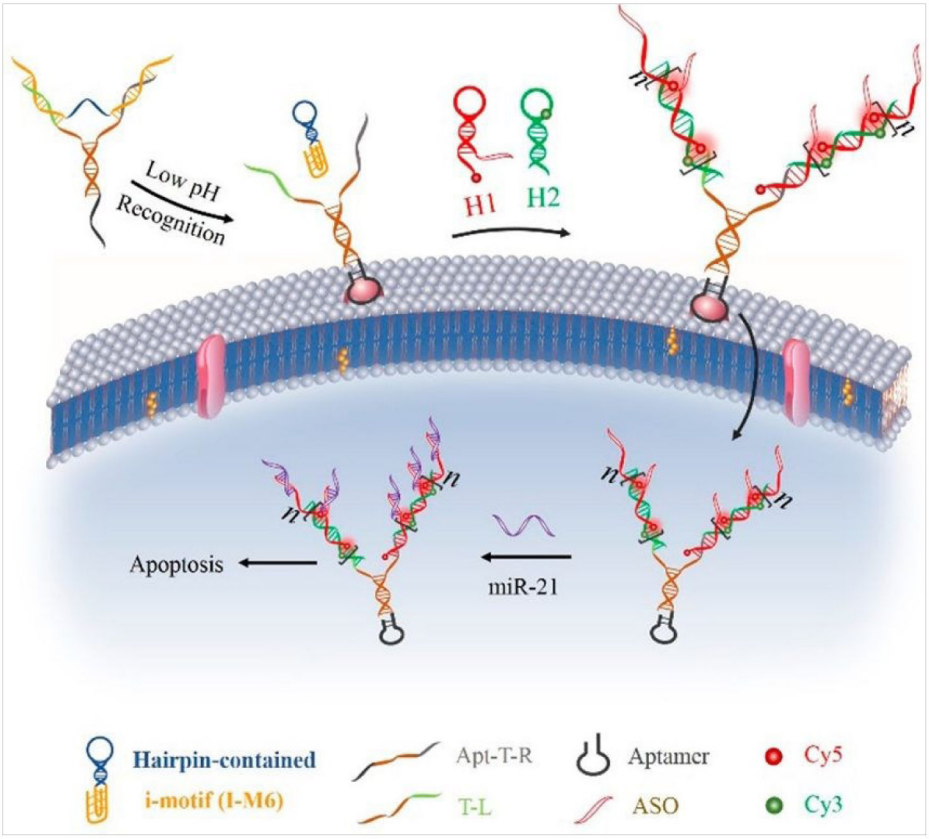

Figure 10.

pH-activatable HCR and siRNA delivery-dual system. The motif first approaches MCF-7 cell membranes with a cell-specific protein aptamer (black). The low pH from the cancerous microenvironment triggers the release of the disguise i-motif is released (yellow-blue), exposing the HCR hairpins on the system. HCR is activated by the T-L strand. An antisense oligonucleotide (pink ASO) is functionalized at the end of one of the HCR hairpins, thus capturing and silencing miR-21 activity. Reprinted (adapted) with permission from No. Copyright 2019 American Chemical Society[26].

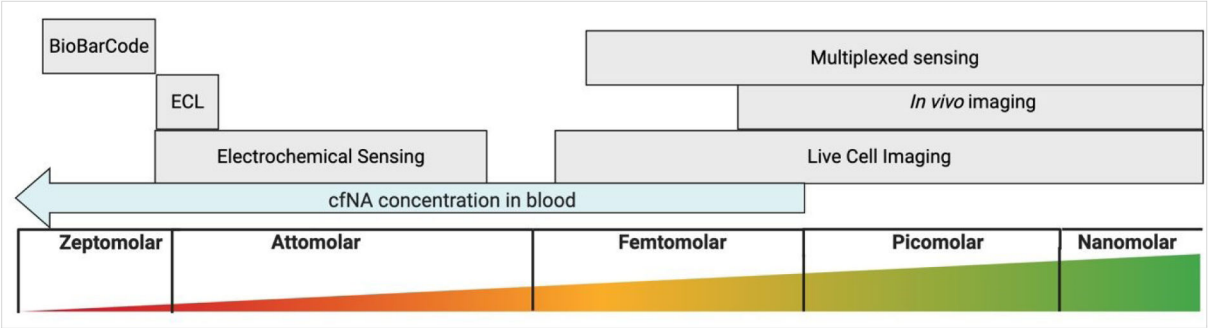

Figure 11:

Current status on nucleic acid detection limits and modalities using strand mediated signal amplification. Electrochemical sensing and ECL remain the most sensitive modes in detection. Multiplexed sensing, though often also reported electrochemically, sacrifices LoD to higher order sensing of diversified targets. Works in imaging are still in the femto- to picomolar level, but they are pushing closer to the estimated abundance of circulation nucleic acid.

Table 1:

Recent strategies that advance live cell imaging through HCR. Limit of detection (within the picomolar to femtomolar range), dynamic range, reaction time (ranging from a few minutes to several hours), and target are specified from the reports. Specificity strategies for sensing efficiency are also outlined. N/R= not reported.

Method	Advantage	LoD	Dynamic Range	Reaction Time	Target	Specificity	Ref
UCNP-conjugated HCR	Spatio-temporal imaging, use of NIR activation	0.6 pM	N/R	1 hr	c-MYCmRNA	Compared with other mRNA and miRNAs	21
Dumbbell structural motifs for HCR	Nuclease resistance, stable up to 16 hours	3.2 pM	25 pM-100 nM	1.5 hr	miR-27a	Single to multi-base mismatch	25
i-motif triggered HCR.	pH-activated imaging	N/R	N/R	5 hr	miR-21	Imaged target negative epithelial cell line	26
Quantum dot-HCR	Brighter fluorescence, spatial imaging	2.78 fM	10 fM-100 pM	N/R	miR-200c-3p	Compared mismatched sequences	54
Click-reaction triggered HCR	Cell glycosylatio n imaging	N/R	N/R	1.5 hr	Sialic acid, galactosamine, glycosylation events	N/R	55
Multiple-aptamer logic device mediated HCR	Boolean logic to accurately sense cell subtype	N/R	N/R	1.5 hr	Tyrosine protein kinaselike 7 (PTK7) and TCOl proteins	Compared across different cell lines	56
3D DNA tetrahedron HCR	70-fold faster imaging	2.14 pM	2-40 pM	20 min	miR-21	One-base mismatch	15
Alkyne-modified HCR to detect azide labeled SiaGcs	Directly quantify SiaGC secretion	N/R	N/R	4 hr	Sialoglycoconju gate (SiaGCs)	N/R	85

Table 2:

Recent strategies that advance live cell imaging through CHA. Limit of detection (within the picomolar to femtomolar range), dynamic range, reaction time (ranging from a few minutes to several hours), and target are specified from the reports. Specificity strategies for sensing efficiency are also outlined. N/R= not reported.

Method	Advantage	LoD	Dynamic Range	Reaction Time	Target	Specificity	Ref
Streptavidin-DNA tetrads for CHA	High contrast in living cells	0.8 pM-0.9 pM	5 pM-1 nM	1.5 hr	Survivin mRNA, TK1 mRNA	Compared to single-and two-based mismatch	14
CHA-mediated nanobrush motif assembly	Image short and long nucleic acid strands	1.03-1.88 nM	5-25 nM	4 hr	miR-21, BRCA1 oncogene DNA	Single and three-base mismatch	53
3D tetrahedron CHA	15.6-fold reaction rate alongside CHA, increased stability	0.15 nM	N/R	48 min	MnSOD mRNA	Tested against different sequences	16
Tetrahedron mediated FRET amplification	9.6 fold faster than traditiona 1 CHA.	3.5 pM	0-10nM	1.5hr	MnSOD mRNA	Single, two and three-based mismatch	101
Genetically encoded fluorescent CHA	High sensitivity and Broccoli incorpora tion for fluoresce nee	2.5 nM	N/R	2 hr	N/R	Compared with different strand sequences	102
Gold nanoparticle-CHA coupled system	Reduction of falsepositive signals, enhanced SNR	3.7 pM	10-1000pM	4hr	miR-21	Compared with miR-41	95

Table 3:

Recent strategies that advance lowered LoD of nucleic acids using HCR. Limit of detection, dynamic range, reaction time, and target are specified from the reports. Specificity strategies for sensing efficiency are also outlined. N/R= not reported.

Method	Signal	LoD	Dynamic Range	SNR	Target	Specificity	Reference
Magnetic networks by HCR	Colorimetric	13 aM	0.05 fM-12 nM	3	let-7a (miRNA)	Compared with let-7b, let-7c and miR-21	57
Nonlinear HCR on bare gold electrodes	Electrochemical	334 aM	1 fM-10 pM	N/R	miRNA-25	Single-base mismatch and other miRNA species	37
Au-immobilized HCR to intercalate RuHex, exonuclease editing	Electrochemical	53 aM	100 aM-100 nM	4.13	miR-122	Single-base mismatch	34
Au-electrode-AuNP HCR sandwich to capture RuHex	Electrochemical	0.68 aM	1 fM-100 fM	3	Helicobact er pylori DNA	Compared with mtDNA, ncDNA, DNA from human serum	25
Ag-nanocluster quenched-ECL via HCR	ECL	4.97 aM	100 aM-1000 pM	3	miRNA-21, thrombin	Thrombin versus AFP, CEA and PSA	40
Gold immobilized DNA tetrahedron base, HCR	Electrochemical	0.93 aM	1 aM-1 pM	N/R	Methylate d DNA	Compared single and multi-base mismatched sequences	36
AuNP@ZnO NCLs	ECL	18.6 aM	100 aM-100 pM	N/R	miRNA-21	Compared with miRNA-122, miRNA-141 and miRNA-155	39
4-arm junction with Fe	Electrochemical	3 aM	10 aM-10 fM	3	miR-21	One-base to multi-base mismatch	58

Table 4:

Recent strategies that advance lowered LoD of nucleic acids using CHA. Limit of detection, dynamic range, reaction time, and target are specified from the reports. Specificity strategies for sensing efficiency are also outlined. N/R= not reported.

Method	Signal	LoD	Dynamic Range	SNR	Target	Specificity	Reference
Bio-bar-coding with CHA	Fluorescence	97.9 zM	10 aM-10 pM	4	miRNA-21	Single and three-base mismatch and complimentary target strand	41
Mesoporous Silica NPs with combined CHA and HCR	Electrochemical	37 aM	N/R	N/R	miR-21	Compared with miRNA 27a, miRNA 375, let-7d, miRNA R-200b	83
NiO@N coupled with CHA	Electrochemical	45 aM	100 aM-100 pM	46.1	Not specified	Tested against single and three-base mismatch sequences	59

Table 5

Recent approaches in optimizing multiplexity within HCR methods.

Method	Signal	LoD	Targets	Max diversity	Specificity	Reference
Branched HCR	Surface acoustic wave sensor (SAW)	25 nM	Not specified	2	N/R	42
CHA on fluorescent microbeads "Luminex xMAP »	fluorescence	2 pM	miRNA-21, miRNA-122, miRNA-222	3 demonstrated ("as many as 500" proposed)	Single-base mismatch and other miRNA species	37
HCR on Photonic Crystals PhCs	Optical (fluorescence)	8fM	miR-21, miR-155, miR210	3	Single-and three-base mismatch	34
Time-gate FRET (TG-FRET)	Photoluminescence	1.7 pM (miRNA) , 0.88 pM (NA)	miR-20a, miR-21	2	Compared with miRNA-20b	25
MERFISH-HCR	fluorescence	N/R	Not specified	130	N/R	40
Magnetic beads with biotin-HCR to capture streptavidin-peroxidase	Electrochemical	0.66 pM	miR-21, let-7a, miR-31	3	Single and double base mismatch, other strands	51
DNA tetrahedron-Y-motif	Fluorescence imaging	7pM (miR-21) 3pM (miRNA-203)	miR-21, miRNA-203	2	Compared with random sequences and nonhomologous RNA	84

Table 6

Recent approaches in optimizing multiplexity within CHA methods.

Method	Signal	LoD	Targets	Max diversity	Specificity	Reference
CHA on fluorescent microbeads "Luminex xMAP »	fluorescence	2 pM	miRNA-21, miRNA-122, miRNA-222	3 demonstrate d ("as many as 500" proposed)	Single-base mismatch and other miRNA species	37
CHA-based gel electrophoresis assay	Gel electrophoresis	lOfM	miRNA-21, miRNA-373, miRNA-lOb	3	Single and double bas mismatch	112

Table 7

Demonstrations on employing strand signal amplification with screening in clinical patient samples. The more popular sample for screening is serum, but urine, tissue, and other samples are useful for HCR and CHA-based sensors.

Sample type	Number of specimens	Signal	Targets and condition	Specificity	Reference
Serum	10	PL intensity	miR-133a, miR-143, miR-200b (bladder cancer)	Tested against sequences with base mutations	50
Serum	10	potentiometric	Matrix-metalloproteinase-7 (MPP7) renal cancer, acute kidney injury	Single-base mismatch and other miRNA species	62
Pleural effusion, serum	25 (P.E), 23 (serum)	Electrochemical	ctDNA (circulating tumor DNA) (hepatocellular carcinoma, breast cancer)	Compared to mismatched DNA sequences, tested with 24 serum samples from healthy individuals	52
Urine	N/R	Dynamic light scattering	Telomerase substrate (TS) (bladder cancer)	Compared with miRNA-20b and urine samples from healthy individuals	63
Tissue (High grade squamous intraepitheli al lesion HSIL)	3	Electrical current	miR-21, let-7a, miR-31 (cervical cancer)	Tested alongside 3 samples from healthy individuals	51
Whole blood	N/R	SAW resonant frequency	N/R	N/R	42